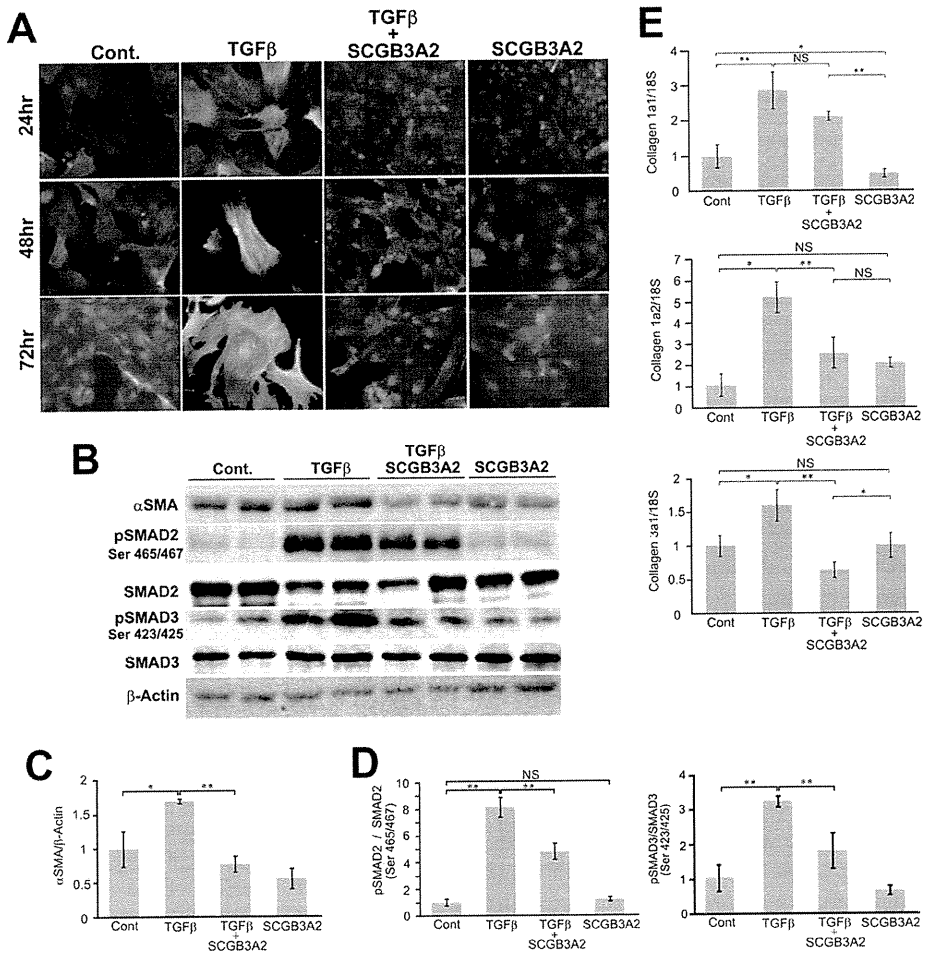

FIGURE 1. **Inhibition of differentiation from fibroblast to myofibroblast by SCGB3A2.** *A*, representative immunocytochemistry for αSMA ($n = 4$) is shown. αSMA was visualized as a *green signal*. Fibroblasts isolated from adult mouse lungs were cultured in the absence (*Cont.*; normal fibroblast) or the presence of SCGB3A2, TGFβ, or TGFβ and SCGB3A2 together for 24–72 h. All the images were taken at ×600 (original magnification). *B*, representative immunoblotting results for αSMA, phosphorylated SMAD2 (*pSMAD2*), total SMAD2, phosphorylated SMAD3 (*pSMAD3*), total SMAD3, and β-actin using cells harvested after 24 h stimulation are shown. *C*, and *D*, densitometric analysis of the immunoblot signals in *B* is shown as the mean ± S.D. ($n = 4$) for αSMA (*C*) and pSMAD2/SMAD2 and pSMAD3/SMAD3 ratios (*D*). *E*, qRT-PCR for collagen 1a1, collagen 1a2, and collagen 3a1 is shown. Fibroblasts were harvested 24 h after stimulation and were subjected to qRT-PCR analysis to determine the level of collagen genes expression. *Cont*, normal fibroblast as control; *TGFβ*, stimulated by TGFβ; *TGFβ+SCGB3A2*, administration of both TGFβ and SCGB3A2; *SCGB3A2*, fibroblast stimulated by SCGB3A2 only. The graph shows the mean ± S.D. from 4–8 lungs per group, each in triplicate. *, $p < 0.05$; **, $p < 0.01$; *NS*, not significant.

did not significantly differ among different culture groups for at least up to 72 h (data not shown). The level of αSMA protein was increased by TGFβ treatment, which returned to control levels in cells treated with SCGB3A2 as determined by Western blotting performed after 24 h of stimulation with TGFβ (Fig. 1, *B* and *C*). SCGB3A2 alone did not have a significant effect on the level of αSMA protein as compared with control. When SMAD2 and SMAD3, the major molecules in the TGFβ signaling pathway, were examined, phosphorylated SMAD2 (*pSMAD2*) and SMAD3 (*pSMAD3*) were increased by TGFβ treatment as expected, and combined treatment with TGFβ and SCGB3A2 partially reversed the increase (Fig. 1, *B* and *D*). Again, SCGB3A2 alone did not have any effect on SMAD2 and SMAD3 phosphorylation. Furthermore, qRT-PCR analysis revealed that the expression of collagen 1a2 and collagen 3a1 was decreased in fibroblasts stimulated by TGFβ and SCGB3A2 together as compared with those treated with TGFβ alone (Fig. 1*E*). Because production of a complete collagen fiber requires three collagens (34), the reduced expression of two collagen genes is likely to account for the reduced Type I and Type III collagen fibers. The effect of SCGB3A2 on the reduced expression of collagen genes was abolished when SCGB3A2 was boiled before the addition to the media, suggesting that the effect of SCGB3A2 was not due to any contaminants in SCGB3A2 preparation (supplemental Fig. S1). These results demonstrated that SCGB3A2 inhibited TGFβ-induced differentiation of primary lung fibroblasts to myofibroblasts.

Induction of STAT1 Phosphorylation and SMAD7 Expression by SCGB3A2—Immunoblotting was performed to examine levels of SMAD7 protein and the status of STAT1 phosphorylation in the presence or absence of TGFβ and/or SCGB3A2 (Fig. 2). It is well documented that IFNγ treatment results in phosphorylation of STAT1 and induces SMAD7 expression, which interferes with the TGFβ signaling (9, 35). In mouse lung primary fibroblasts, the expression of SMAD7, STAT1, and phosphorylated STAT1 was hardly detectable in control and TGFβ-

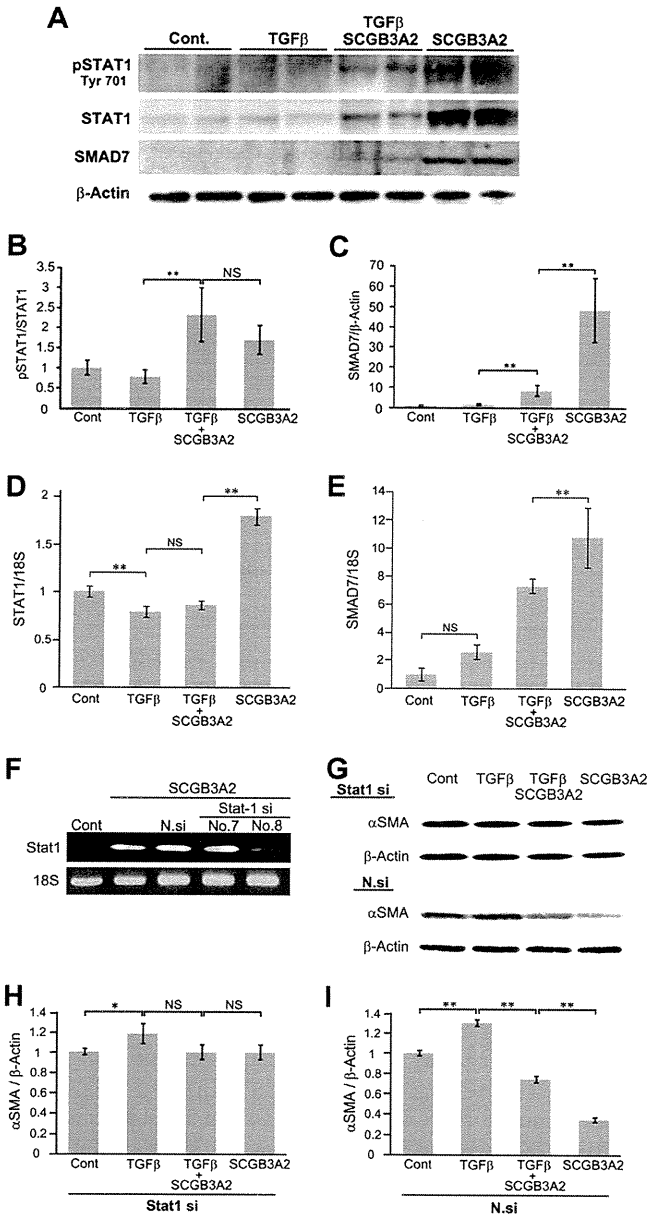

FIGURE 2. **Phosphorylation of STAT1 and SMAD7 expression by SCGB3A2.** *A*, immunoblotting for phosphorylated STAT1 (*pSTAT1*), total STAT1, SMAD7, and β-actin as control is shown. *B* and *C*, shown is a graph for densitometric analysis of the immunoblot signals shown in *A* for pSTAT1/STAT1 (*B*) and SMAD7/β-actin (*C*). The mean ± S.D. ($n = 4$) is shown. *D* and *E*, qRT-PCR for STAT1 (*D*) and SMAD7 (*E*) using 18 S as an internal control is shown. *NS*, not significant. *F–I*, effect of STAT1 siRNA or nonspecific control siRNA on the level of αSMA is shown. *F*, qRT-PCR to confirm knockdown of STAT1 mRNA with STAT1 siRNA probes is shown. *G*, immunoblotting for αSMA and β-actin using cells transfected with no. 8-STAT1 siRNA probe (*STAT1 si*) or nonspecific negative siRNA probe (*N.si*). *H* and *I*, shown is a graph for densitometric analysis of the immunoblot signals shown in *G* for αSMA/β-actin with a STAT1 siRNA probe (*H*) and nonspecific negative siRNA probe (*I*). The mean ± S.D. ($n = 4$) is shown. Fibroblasts were harvested 24 h after stimulation. *Cont*, normal fibroblast as control; *TGFβ*, stimulated by TGFβ; *TGFβ+SCGB3A2*, administration of both TGFβ and SCGB3A2; *SCGB3A2*, fibroblast stimulated by SCGB3A2 only. **, $p < 0.01$, *NS*, not significant. Representative immunoblotting results are shown.

treated cells (Fig. 2*A*). In contrast, the level of STAT1, phosphorylated STAT1 (pSTAT1), and SMAD7 was markedly increased when fibroblasts were treated with SCGB3A2 (Fig. 2, *A–C*). TGFβ dramatically inhibited the induction of STAT1 and SMAD7 by SCGB3A2 (see *TGFβ+SCGB3A2 versus SCGB3A2*), whereas the pSTAT1/STAT1 ratio stayed at similar levels with TGFβ+SCGB3A2 and SCGB3A2-only treatments (Fig. 2*B*). The SCGB3A2-induced increase of STAT1 and SMAD7 expression was due to an mRNA increase as demonstrated by qRT-PCR (Fig. 2, *D* and *E*, respectively). When STAT1 siRNA was transfected to mouse lung primary fibroblasts followed by treatment with TGFβ and/or SCGB3A2, TGFβ-induced αSMA expression levels stayed the same with and without SCGB3A2 (Fig. 2, *G* and *H*). With control nonspecific negative siRNA, TGFβ-induced αSMA expression was reduced by SCGB3A2 as expected (Fig. 2*I*), confirming that the effect of SCGB3A2 is through STAT1. These data demonstrated that SCGB3A2 enhanced expression of SMAD7 and STAT1 and phosphorylation of STAT1, resulting in inhibition of the TGFβ signaling pathway.

Relationship between SCGB3A2 and Interferon γ Receptor—Several cytokines are known to activate STAT1. Among them, the key cytokine that activates STAT1 is IFNγ (36). IFNγ is known to improve fibrosis through phosphorylation of STAT1 (5, 6, 12), and its clinical effect on pulmonary fibrosis is well documented (37). IFNα and IFNβ also activate STAT1 and inhibit fibrosis (38–40). RT-PCR analysis using lung primary fibroblasts demonstrated that IFNγ was not expressed in lung primary fibroblasts regardless of SCGB3A2 treatment (Fig. 3*A*). Similarly, neither IFNα nor IFNβ was expressed in lung primary fibroblasts stimulated by SCGB3A2 (supplemental Fig. S2). In the following studies, we focused on the relationship between SCGB3A2 and IFNγ and its receptor. When IFNγ receptor-specific neutralizing antibody was added to the culture, IFNγ-induced phosphorylation of STAT1 was inhibited, whereas it did not inhibit phosphorylation of STAT1 induced by SCGB3A2 (Fig. 3*B*). Interestingly, it took ~3 h for the SCGB3A2-induced phosphorylation of STAT1 to reach maximum levels (Fig. 3*C*). This was unusually long as compared with the IFNγ-induced STAT1 phosphorylation, which reached maximal levels within 30 min of stimulation (41, 42) (supplemental Fig. S3). Furthermore, SCGB3A2-stimulated STAT1 phosphorylation was suppressed in the presence of CHX (Fig. 3*D*). In contrast, IFNγ-stimulated STAT1 phosphorylation was unchanged with and without CHX treatment (Fig. 3*E*). These data indicated that SCGB3A2 promoted phosphorylation of STAT1 in a manner independent of IFNγ receptor and through a CHX-sensitive intermediate molecule. These data further suggested that the SCGB3A2-STAT1 signaling may have been through a SCGB3A2-specific receptor.

Inhibition of BLM-induced Lung Fibrosis by SCGB3A2—To validate these *in vitro* data that SCGB3A2 suppresses the TGFβ signaling pathway resulting in reduction of fibrosis, mice were subjected to a pulmonary fibrosis model. Pulmonary fibrosis was induced by direct administration of BLM or PBS as control to mice by intratracheal intubation. The histopathology of the lungs on day 14 (2 weeks) after BLM treatment did not reveal any fibrosis regardless of treatment regimens (data not shown). At day 14, mice received the first of 7 daily consecutive intravenous injections of SCGB3A2 or PBS through the tail vein (Fig. 4*A*). On day 21 after BLM administration, pulmonary fibrosis

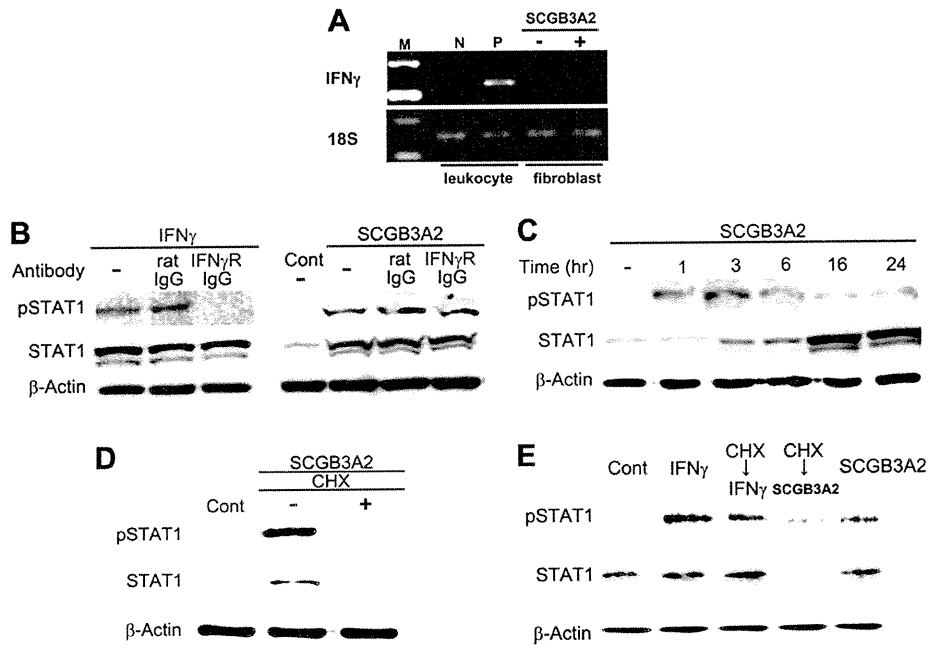

FIGURE 3. **Relationship between SCGB3A2 and IFNγ receptor.** *A*, representative RT-PCR for IFNγ in fibroblasts in the presence or absence of SCGB3A2 (n = 3) is shown. Leukocytes stimulated by phorbol 12-myristate 13-acetate (10 ng/ml) and ionomycin (1 μM) for 3 h were used as a positive control for IFNγ. *B*, shown are blocking experiments for IFNγ receptor signaling. A representative result is shown (n = 3). pSTAT1 was detected in the presence of anti-IFNγ receptor antibody and SCGB3A2 (*right panel*). *C*, a representative time-course result of STAT1 phosphorylation by SCGB3A2 (n = 3) is shown. *D* and *E*, protein synthesis blocking experiments are shown. Fibroblasts were incubated with both SCGB3A2 and CHX (1 μg/ml) for 3 h (*D* and *E* for CHX→SCGB3A2) or were preincubated with CHX (1 μg/ml) for 3 h before stimulation with IFNγ for 15 min (*E*). A representative result is shown (n = 3).

was observed in the lungs of BLM-treated group of mice (Group 1). The extent of fibrosis was rated as grade 1 to grade 2 (Fig. 4*B*). In contrast, mice in Group 2 that received BLM and SCGB3A2 did not develop any pulmonary fibrosis except one mouse of five tested. In Group 3, one mouse exhibited small fibrotic lesions, whereas no fibrosis was observed in Group 4 mice. Collagen fibers were found to focally occupy the alveolar space of mice in Group 1 but not in other groups of lungs as determined by Masson's Trichrome staining, which detects collagen fibers (Fig. 4*C*, *upper panel*). Excessive SCGB3A2 expression was focally found in a part of airway epithelial cells and the foci of fibrosis of Group 1 mouse lungs (Fig. 4*C*, *lower panel*). In contrast, other groups of lungs (Groups 2–4) expressed SCGB3A2 at similar levels in airway epithelial cells as expected, although Group 2 lungs appeared to have slightly higher expression than Group 3 and 4 lungs. When the expression of total SAMD2/3 as well as pSMAD2 and pSMAD3 was examined by immunohistochemistry, all were highly up-regulated in most of airway epithelial cells as well as the foci of fibrosis in Group 1 mouse lungs, whereas expression stayed at similar levels and patterns in other groups of lungs including those of BLM+SCGB3A2 administered mouse lungs (Group 2) (supplemental Fig. S4). The latter results suggested that SCGB3A2 appeared to have suppressed expression of SMAD2/3 and/or pSMAD2 and pSMAD3 in epithelial as well as parenchymal cells. The numbers of macrophages and neutrophils in BALF were enhanced by BLM treatment, whereas they were markedly reduced to levels close to that of controls in the SCGB3A2-treated group (Fig. 4*D*). The number of lymphocytes was not different with statistical significance among the four groups (data not shown). These data indicated that development of BLM-induced fibrosis was suppressed by the daily administration of SCGB3A2 on the third week of BLM treatment.

Alteration of Gene Expression by BLM and/or SCGB3A2—To determine the genes whose expression was altered in the BLM-induced lung fibrosis and/or SCGB3A2-induced reduction of fibrosis, microarray analysis was carried out using mRNAs obtained from lungs of mice between Group 1 (BLM-treated) and Group 3 (PBS control) and Group 1 (BLM-treated) and Group 2 (BLM- and SCGB3A2-treated). With a cutoff of >1.5-fold change in expression, 1646 and 1275 genes were, respectively, up- and down-regulated by BLM as compared with control PBS (between Group 1 and Group 3), and 346 and 919 genes were, respectively, up- and down-regulated by SCGB3A2 treatment as compared with no SCGB3A2 treatment in BLM treated mice (between Group 1 and Group 2). Using these genes, GO (gene ontology) analysis was performed for the changes caused by BLM and for the effect of SCGB3A2 in BLM-treated mice (heat map results are shown in supplemental Fig. S5). The results revealed that "Inflammatory response" and "Response to wounding" under "Biological Process" and "Extracellular region part," "Extracellular region," and "Extracellular space" under "Cellular Component" were overexpressed by BLM injury (Table 1) and suppressed by administration of SCGB3A2 (Table 2). Additionally, to demonstrate genes that are altered by SCGB3A2, microarray analysis was carried out using lung RNAs of normal mice that were intravenously administered SCGB3A2 and were euthanized 12 h later. GO analysis revealed that "Signal transducer activity" and "Molec-

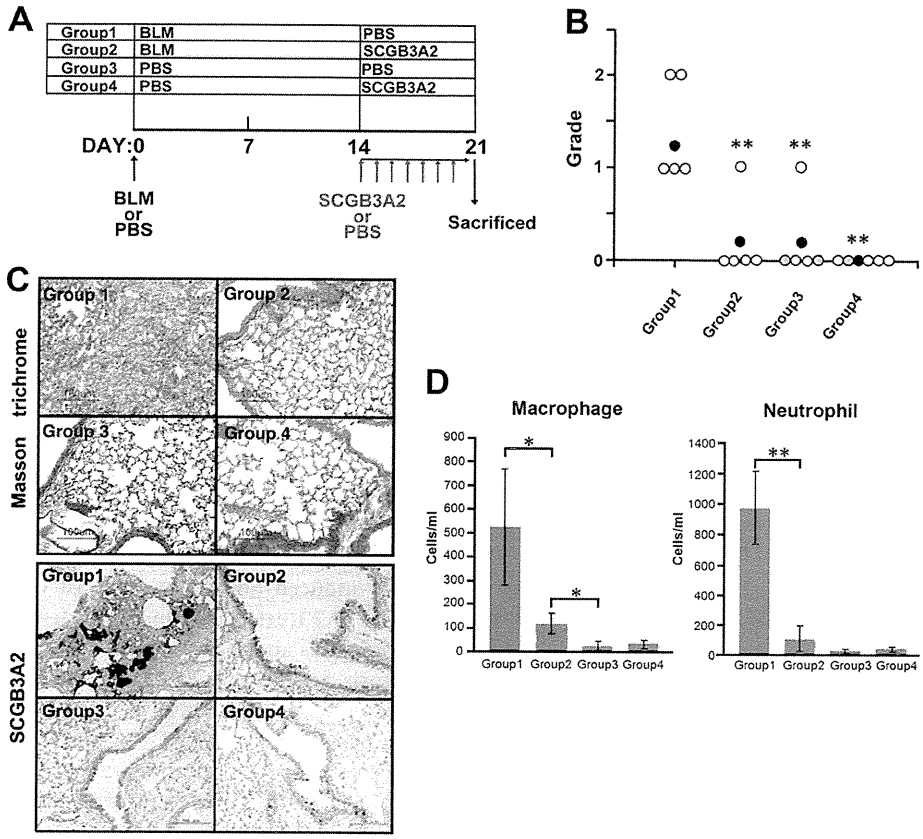

FIGURE 4. **Inhibition of BLM-induced lung fibrosis by SCGB3A2.** *A*, shown is a scheme to prepare BLM-induced fibrosis model mice. BLM or PBS was administered to the lungs of C57BL/6N mice by intratracheal intubation at day 0. SCGB3A2 or PBS was administered to mice by intravenous injection once daily for a week starting at day 14 followed by euthanasia at day 21. The four groups of mice were subjected to the studies as shown. PBS was administered as a control in Groups 3 and 4. Whole experiments were carried out at least twice. *B*, grading of fibrosis carried out as described under "Experimental Procedures." BLM administration resulted in production of fibrous tissue, focally or diffusely in lungs of Group 1, whereas no fibrous tissue formation was observed in four of five lungs exposed to BLM followed by SCGB3A2 treatment in Group 2. *White circle*, no lesions; *black circle*, mean ($n = 5$); *gray*, presence of a few infiltrating foci of lymphocytes or very small granulomas. **, $p < 0.01$, Group 1 *versus* Groups 2, 3, or 4. *C*, Masson's Trichrome staining and immunohistochemistry for SCGB3A2 are shown. Collagen fibers were focally detected as a blue color by Masson trichrome staining in the parenchyma of the lungs of mice in Group 1 but not the lungs of other groups. Excessive SCGB3A2 expression was found in a part of the epithelial cells and in the foci of fibrosis as a brown color by immunohistochemistry in Group 1. Representative staining is shown ($n = 5$). *D*, shown are the number of macrophages and neutrophils in BALF. The number of macrophages and neutrophils increased by BLM (*Group 1*) was significantly decreased by administration of SCGB3A2 (*Group 2*), especially neutrophils which reduced to the levels of control (*Group 3* and *Group 4*). The graph shows the mean ± S.D. from 5 lungs per group ($n = 5$). *, $p < 0.05$; **, $p < 0.01$.

ular transducer activity" categorized by only one term "Molecular Function" were up-regulated by short-term treatment of SCGB3A2 (Table 3). The TGFβ signaling was among the top pathways identified by the Pathway Mapping program (Fig. 5), further supporting our conclusion that SCGB3A2 affects the TGFβ signaling pathway.

Further analysis revealed that the expression of matrix metalloproteinases (MMPs) and other extracellular matrix (ECM)-degrading enzymes that degrade damaged tissues as well as enzymes synthesizing collagen I, fibronectin, hyaluronic acid, and other components of wound provisional ECM was altered after BLM and/or SCGB3A2 treatment (supplemental Table S2). qRT-PCR was performed to confirm the alterations of gene expression in BLM-treated lungs with (Group 2) and without (Group 1) SCGB3A2 (Fig. 6). High levels of MMP2, MMP12, and MMP14 expression in BLM-treated lungs (Group 1) were significantly decreased by the administration of SCGB3A2 (Group 2); in particular, MMP14 returned to the levels of the "no BLM treatment" groups (Group 3 and 4). Cathepsin S and D that belong to a group of proteinases were also highly expressed in BLM-treated group (Group 1), and decreased to a level similar to control by SCGB3A2 (Group 2). Cathepsin C levels did not show any statistically significant difference among the four groups of mice. These data further indicated a role for SCGB3A2 in suppression of lung fibrosis induced by BLM.

DISCUSSION

This study revealed that SCGB3A2 possesses anti-fibrotic activity as revealed by *in vitro* cell culture studies with primary lung fibroblasts and *in vivo* studies using a BLM-induced pulmonary fibrosis model mouse. SCGB3A2, a member of the SCGB gene superfamily composed of secretory proteins of small molecular weight, is predominantly expressed in lung airways (14, 43). The most studied member of the SCGB gene superfamily, namely SCGB1A1, also called uteroglobin, Clara cell 10-kDa protein, or Clara cell secretory protein, is a multifunctional protein with anti-inflammatory/immunomodulatory properties with manifestation of antichemotactic, antiallergic, antitumorigenic, and embryonic growth-stimulatory activities (19). The current study revealed that the related pro-

TABLE 1
GO terms for overexpressed genes in BLM-injured lung

Gene ontology term	Cluster frequency[a]	Total frequency[b]	Corrected p value[c]
	%	%	
Biological Process, cell adhesion	6.40	3.50	2.92×10^{-5}
Biological adhesion	6.40	3.50	2.92×10^{-5}
Antigen processing and presentation of exogenous peptide antigen	0.70	0.10	0.00654
Immune system process	6.30	3.90	0.01711
Inflammatory response	2.70	1.30	0.01977
Antigen processing and presentation of peptide antigen via MHC class II	0.60	0.10	0.02221
Antigen processing and presentation of exogenous peptide antigen via MHC class II	0.60	0.10	0.02221
Antigen processing and presentation of peptide of polysaccharide antigen via MHC class II	0.60	0.10	0.04108
Response to wounding	3.30	1.80	0.04663
Cellular Component			
Extracellular region part	18.00	12.70	5.62×10^{-7}
Extracellular matrix	4.00	1.70	1.05×10^{-6}
Proteinaceous extracellular matrix	3.39	1.70	1.68×10^{-6}
Extracellular region	20.40	15.10	5.57×10^{-6}
Extracellular space	16.80	12.00	7.62×10^{-6}
Molecular function			
Carbohydrate binding	3.00	1.60	0.04087

[a] Frequency of Entrez Gene IDs appeared in a given GO term based on those having over 0.585 in log ratio.
[b] Frequency of Entrez Gene IDs appeared in a given GO term based on all genes.
[c] p value corrected using the Bonferroni method.

TABLE 2
GO terms for suppressed genes by SCGB3A2 in BLM-injured lung

Gene ontology term	Cluster frequency[a]	Total frequency[b]	Corrected p value[c]
	%	%	
Biological process			
Defense response	6.10	2.50	6.78×10^{-5}
Response to external stimulus	6.40	2.70	7.91×10^{-5}
Response to wounding	4.50	1.80	0.00172
Response to stimulus	15.80	10.60	0.00896
Inflammatory response	3.20	1.30	0.03692
Cellular component			
Extracellular region	24.50	15.10	1.82×10^{-9}
Extracellular region part	20.40	12.70	2.26×10^{-7}
Extracellular space	19.50	12.00	3.22×10^{-7}

[a] Frequency of Entrez Gene IDs appeared in a given GO term based on those having over 0.585 in log ratio.
[b] Frequency of Entrez Gene IDs appeared in a given GO term based on all genes.
[c] p value corrected using the Bonferroni method.

TABLE 3
GO terms overexpressed by SCGB3A2 in normal lung

Gene ontology term, molecular function	Cluster frequency[a]	Total frequency[b]	Corrected p value[c]
	%	%	
Signal transducer activity	20.7	15.9	0.0378
Molecular transducer activity	20.7	15.9	0.0378

[a] Frequency of Entrez Gene IDs appeared in a given GO term based on those having over 0.585 in log ratio.
[b] Frequency of Entrez Gene IDs appeared in a given GO term based on all genes.
[c] p value corrected using the Bonferroni method.

tein SCGB3A2 at therapeutic levels has novel biological activity toward induced fibrosis in addition to its known anti-inflammatory (24) and growth factor activities (25). SCGB1A1 was previously suggested to be a novel cytokine (44). The current results support the notion that the SCGB gene superfamily may be a novel cytokine family. The anti-inflammatory, growth factor and anti-fibrotic activities that SCGB3A2 possesses may suggest a potential use for this protein in the treatment of many lung diseases, including lung fibrosis as demonstrated in this study.

BLM administered by intratracheal intubation induced pulmonary fibrosis, which focally occupied the pulmonary parenchyma by 3 weeks after BLM administration. Interestingly, BLM-induced fibrosis was almost completely suppressed by SCGB3A2 treatment, which interfered with the infiltration of neutrophils and macrophages into lung and the expression of fibrosis related-genes such as collagens, fibronectin, elastin, cathepsins, and MMPs, all of which were up-regulated by BLM. The development of fibrosis was hardly detectable by the end of 2 weeks after BLM administration, suggesting that SCGB3A2 might inhibit development of fibrosis when given at its early stages.

The anti-fibrotic activity of SCGB3A2 appears to be exerted through STAT1 phosphorylation, induction of SMAD7, and inhibition of SMAD2/3 phosphorylation, which results in suppression of the TGFβ signaling, ultimately leading to the inhibition of myofibroblasts formation. Interestingly, this is the exact pathway that IFNγ exhibits its anti-fibrotic activity (9, 35). We initially hypothesized that SCGB3A2 may induce the expression of IFNγ, thereby suppressing TGFβ signaling. However, the SCGB3A2 pathway is likely to be distinct from the IFNγ pathway based on the following reasons; 1) IFNγ-induced phosphorylation of STAT1 and increased expression of SMAD7 usually occurs within 10–30 min after IFNγ stimulation (supplemental Fig. S3) (9, 41, 42, 45), whereas it took ~3 h for SCGB3A2 to induce maximum levels of STAT1 phosphorylation, 2) SCGB3A2 did not induce IFNγ mRNA expression as determined by RT-PCR, 3) IFNγ receptor neutralizing antibody (46) did not block SCGB3A2-induced STAT1 phosphorylation, and 4) CHX ablated the expression of pSTAT1 in fibroblasts treated with SCGB3A2 but not IFNγ. These results suggest the involvement of a newly synthesized protein upon SCGB3A2 stimulation other than IFNγ in the SCGB3A2-pSTAT1 pathway. In this regard it is interesting to note that STAT1 was induced by SCGB3A2 in a CHX-sensitive fashion. SMAD7 was also induced by SCGB3A2. The SCGB3A2-induced increase of STAT1 and SMAD7 expression was dramatically inhibited by TGFβ at the mRNA levels. However the pSTAT1/STAT1 ratio stayed the same. The involvement of STAT1 in the SCGB3A2 pathway was confirmed by STAT1 siRNA experiments, in which no decrease of αSMA was observed in

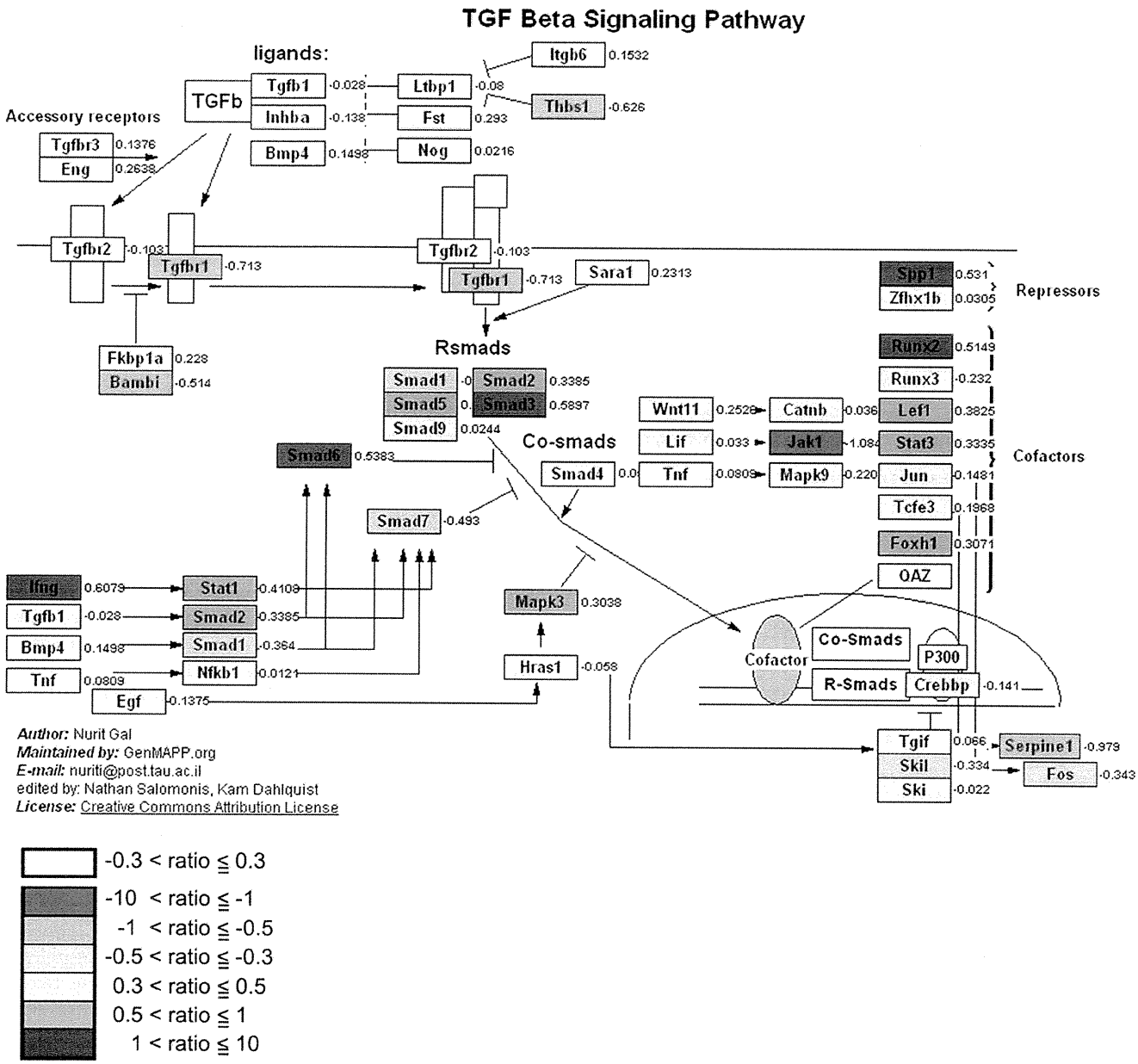

FIGURE 5. **Effect of SCGB3A2 on TGFβ signaling pathway.** Pathway analysis of microarray data showed that the TGFβ signaling pathway was affected by administration of SCGB3A2. Median -fold differences from seven separate samples for each gene on which microarray analysis were run are color-coded based on the *scale* shown at the *bottom left*.

TGFβ+SCGB3A2-treated cells as compared with TGFβ only treatment. These results together suggest that the SCGB3A2-pSTAT1-SMAD7 signaling pathway may be through a SCGB3A2-specific receptor that is distinct from the IFNγ receptor (Fig. 7). We previously suggested the presence of a SCGB3A2-specific receptor-like molecule on the surface of pulmonary mesenchymal cells (25). The nature of the CHX-sensitive intermediate molecule(s), a SCGB3A2-specific receptor, and the mechanism(s) for the inhibitory effect of TGFβ on the induction of STAT1 and SMAD7 by SCGB3A2 are currently not known. Further experiments are required to address these questions. Other cytokines/molecules such as IFNα, IFNβ, epidermal growth factor, growth hormone, and estrogen are known to activate STAT1 (47). Among them, neither IFNα nor IFNβ was induced by SCGB3A2 in mouse lung primary fibroblasts, suggesting that they are not likely involved in the SCGB3A2-pSTAT1-SMAD7 pathway. The involvement of the other cytokines/molecules in the SCGB3A2-pSTAT1 pathway needs to be examined.

Inflammation is the first to occur after BLM administration followed by fibrosis (3–6). In animal models the fibrosis stage starts ~1 week after BLM administration (3). In our BLM model, SCGB3A2 was administered at the fibrosis period and exhibited anti-fibrotic activity through blocking the TGFβ signaling pathway. We previously demonstrated using mice-exogenously administered SCGB3A2 that SCGB3A2

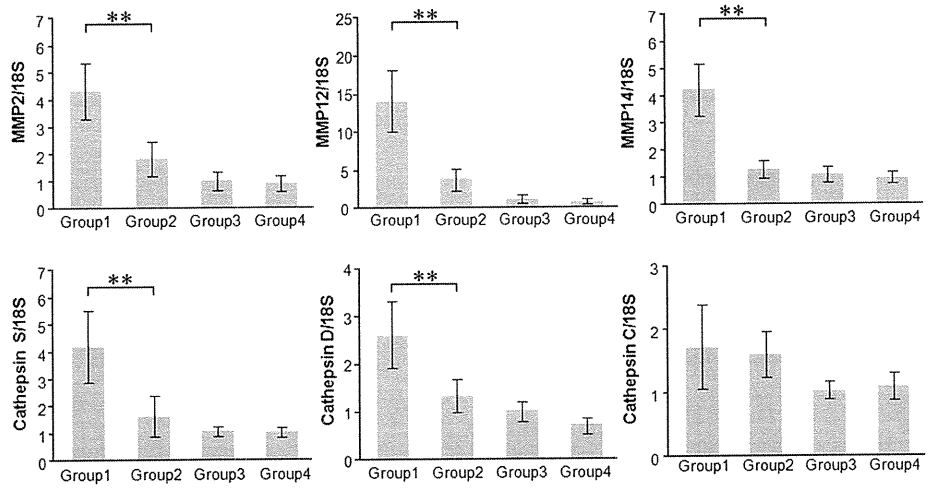

FIGURE 6. **Confirmation of microarray data by qRT-PCR.** Expression levels of MMP2, MMP12, MMP14, cathepsin S, cathepsin D, and cathepsin C mRNAs relative to 18 S were determined by qRT-PCR using mRNAs prepared from mouse lungs of Groups 1–4 as described in Fig. 4. The *graph* shows the mean ± S.D. from 4–9 lungs per group, each in triplicate. **, $p < 0.01$.

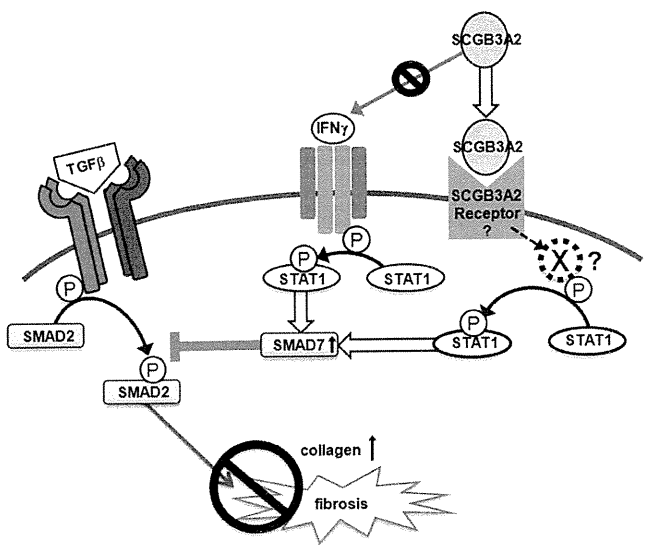

FIGURE 7. **Schematic diagram for the SCGB3A2-induced inhibition of the TGFβ signaling pathway.** SCGB3A2 inhibits collagen production through STAT1 phosphorylation and increases expression of SMAD7, which inhibits TGFβ-mediated SMAD2/3 activation. A newly synthesized molecule *X* mediates the SCGB3A2-induced STAT1 phosphorylation.

exhibits anti-inflammatory activities. We do not know whether SCGB3A2, if administered at the beginning of BLM administration, exerts anti-inflammatory activities and reduces the damage otherwise caused by BLM. Furthermore, we do not know whether endogenous SCGB3A2 regulates pulmonary inflammation and/or fibrosis. However, the following evidence suggests a role for SCGB3A2 in inflammation in lung *in vivo*; in the ovalbumin-induced allergic airway inflammation model mouse, SCGB3A2 expression is reduced in the airways (24, 48, 49), and the plasma SCGB3A2 levels are significantly lower in severe asthmatics without oral corticosteroid treatment as compared with mild- or moderate-asthma patients and controls (50). In the current study, a rather strong focal SCGB3A2 expression was found in a part of epithelial cells, and overexpressed SCGB3A2 was accumulated in fibrotic foci of lungs of mice subjected to BLM. However, it should be noted that these lungs are already at late stages, having developed BLM-induced fibrosis. In BLM+SCGB3A2-treated lungs, SCGB3A2 expression is in similar patterns but is slightly up-regulated to those found in control mice. Whether SCGB3A2 is down-regulated right after BLM administration needs to be determined.

Although IFNγ has been used as a therapy for pulmonary fibrosis (5, 6, 12), it causes a number of potentially harmful side effects and thus is not useful for advanced fibrosis (nlm.nih.gov (13)). In this study SCGB3A2 signaling was found to cross-talk with the IFNγ except at the beginning of the pathway. This suggests that SCGB3A2 could be potentially useful in treating fibrosis, in particular pulmonary fibrosis. More importantly, SCGB3A2 can be administered intratracheally. SCGB3A2 is almost exclusively expressed in lung (14) and is present at relatively high levels in the BALF of normal lungs (24). Thus, delivering a protein into a place where the protein is naturally present in high amounts would probably not cause toxicities. Alternatively, SCGB3A2 can be administered intravenously. Indeed, SCGB3A2 growth factor activity was previously demonstrated *in vivo* by intravenous administration of SCGB3A2 to pregnant female mice through the tail vein resulting in advanced development of fetal lungs (25). In that study, no gross abnormalities were observed in any fetal organs after intravenous SCGB3A2 administration. Furthermore, histological examination of the dam's lung did not show any abnormalities. Based on these facts, it is likely that SCGB3A2 may potentially improve pulmonary fibrosis without harmful side effects as seen with IFNγ. It is possible that BLM treatment as a chemotherapy reagent may not damage the lung if SCGB3A2 is given at the same time. However, additional studies are necessary to determine the efficacy of SCGB3A2 in treating pulmonary fibrosis in humans.

In conclusion, the present study demonstrated that SCGB3A2 inhibits TGFβ signaling through increased STAT1 phosphorylation and expression of SMAD7 and decreased phosphorylation of SMAD2/3, leading to inhibition of myofi-

broblast differentiation. The inhibitory effect of SCGB3A2 on myofibroblast differentiation was reproduced using a BLM-induced lung fibrosis model mouse, in which the severity of lung fibrosis was reduced by SCGB3A2 administration.

Acknowledgments—We thank Drs. Lalage Wakefield, Kathleen Flanders, and Frank Gonzalez (NCI, National Institutes of Health) for advice and critical review of the manuscript and Michie Kobayashi for microarray analysis (DNA Chip Research Inc., Yokohama, Japan).

REFERENCES

1. Coultas, D. B., Zumwalt, R. E., Black, W. C., and Sobonya, R. E. (1994) *Am. J. Resp. Crit. Care Med.* **150,** 967–972
2. Crystal, R. G., Bitterman, P. B., Mossman, B., Schwarz, M. I., Sheppard, D., Almasy, L., Chapman, H. A., Friedman, S. L., King, T. E., Jr., Leinwand, L. A., Liotta, L., Martin, G. R., Schwartz, D. A., Schultz, G. S., Wagner, C. R., and Musson, R. A. (2002) *Am. J. Respir. Crit. Care Med.* **166,** 236–246
3. Moeller, A., Ask, K., Warburton, D., Gauldie, J., and Kolb, M. (2008) *Int. J. Biochem. Cell Biol.* **40,** 362–382
4. Cutroneo, K. R., White, S. L., Phan, S. H., and Ehrlich, H. P. (2007) *J. Cell. Physiol.* **211,** 585–589
5. Tzortzaki, E. G., Antoniou, K. M., Zervou, M. I., Lambiri, I., Koutsopoulos, A., Tzanakis, N., Plataki, M., Maltezakis, G., Bouros, D., and Siafakas, N. M. (2007) *Respir. Med.* **101,** 1821–1829
6. Wynn, T. A. (2004) *Nat. Rev. Immunol.* **4,** 583–594
7. Eickelberg, O., Pansky, A., Koehler, E., Bihl, M., Tamm, M., Hildebrand, P., Perruchoud, A. P., Kashgarian, M., and Roth, M. (2001) *FASEB J.* **15,** 797–806
8. Ghosh, A. K., and Varga, J. (2007) *J. Cell. Physiol.* **213,** 663–671
9. Ulloa, L., Doody, J., and Massagué, J. (1999) *Nature* **397,** 710–713
10. Zhang, S., Fei, T., Zhang, L., Zhang, R., Chen, F., Ning, Y., Han, Y., Feng, X. H., Meng, A., and Chen, Y. G. (2007) *Mol. Cell Biol.* **27,** 4488–4499
11. Scotton, C. J., and Chambers, R. C. (2007) *Chest* **132,** 1311–1321
12. Puente, N. A., Aliotta, J. M., and Passero, M. A. (2007) *Med. Health R. I.* **90,** 43–45
13. Selman, M. (2003) *Am. J. Respir. Crit. Care Med.* **167,** 945–946
14. Niimi, T., Keck-Waggoner, C. L., Popescu, N. C., Zhou, Y., Levitt, R. C., and Kimura, S. (2001) *Mol. Endocrinol.* **15,** 2021–2036
15. Reynolds, S. D., Reynolds, P. R., Pryhuber, G. S., Finder, J. D., and Stripp, B. R. (2002) *Am. J. Respir. Crit. Care Med.* **166,** 1498–1509
16. Klug, J., Beier, H. M., Bernard, A., Chilton, B. S., Fleming, T. P., Lehrer, R. I., Miele, L., Pattabiraman, N., and Singh, G. (2000) *Ann. N.Y. Acad. Sci.* **923,** 348–354
17. Shijubo, N., Kawabata, I., Sato, N., and Itoh, Y. (2003) *Curr. Pharm. Des.* **9,** 1139–1149
18. Wang, S. Z., Rosenberger, C. L., Bao, Y. X., Stark, J. M., and Harrod, K. S. (2003) *J. Immunol.* **171,** 1051–1060
19. Mukherjee, A. B., Zhang, Z., and Chilton, B. S. (2007) *Endocr. Rev.* **28,** 707–725
20. Mandal, A. K., Zhang, Z., Ray, R., Choi, M. S., Chowdhury, B., Pattabiraman, N., and Mukherjee, A. B. (2004) *J. Exp. Med.* **199,** 1317–1330
21. Miele, L. (2000) *Ann. N.Y. Acad. Sci.* **923,** 128–140
22. Watson, M. A., and Fleming, T. P. (1996) *Cancer Res.* **56,** 860–865
23. Culleton, J., O'Brien, N., Ryan, B. M., Hill, A. D., McDermott, E., O'Higgins, N., and Duffy, M. J. (2007) *Int. J. Cancer* **120,** 1087–1092
24. Chiba, Y., Kurotani, R., Kusakabe, T., Miura, T., Link, B. W., Misawa, M., and Kimura, S. (2006) *Am. J. Respir. Crit. Care Med.* **173,** 958–964
25. Kurotani, R., Tomita, T., Yang, Q., Carlson, B. A., Chen, C., and Kimura, S. (2008) *Am. J. Respir. Crit. Care Med.* **178,** 389–398
26. Bin, L. H., Nielson, L. D., Liu, X., Mason, R. J., and Shu, H. B. (2003) *J. Immunol.* **171,** 924–930
27. Maeng, H. G., Lim, H., Jeong, Y. J., Woo, A., Kang, J. S., Lee, W. J., and Hwang, Y. I. (2009) *Immunobiology* **214,** 311–320
28. Lin, Y. C., Huang, D. Y., Chu, C. L., and Lin, W. W. (2010) *Mol. Immunol.* **47,** 1569–1578
29. Asazuma-Nakamura, Y., Dai, P., Harada, Y., Jiang, Y., Hamaoka, K., and Takamatsu, T. (2009) *Exp. Cell Res.* **315,** 1190–1199
30. Kurotani, R., Yoshimura, S., Iwasaki, Y., Inoue, K., Teramoto, A., and Osamura, R. Y. (2002) *J. Endocrinol.* **172,** 477–487
31. Ashburner, M., Ball, C. A., Blake, J. A., Botstein, D., Butler, H., Cherry, J. M., Davis, A. P., Dolinski, K., Dwight, S. S., Eppig, J. T., Harris, M. A., Hill, D. P., Issel-Tarver, L., Kasarskis, A., Lewis, S., Matese, J. C., Richardson, J. E., Ringwald, M., Rubin, G. M., and Sherlock, G. (2000) *Nat. Genet.* **25,** 25–29
32. Doniger, S. W., Salomonis, N., Dahlquist, K. D., Vranizan, K., Lawlor, S. C., and Conklin, B. R. (2003) *Genome Biol.* **4,** R7
33. Tomasek, J. J., Gabbiani, G., Hinz, B., Chaponnier, C., and Brown, R. A. (2002) *Nat. Rev. Mol. Cell Biol.* **3,** 349–363
34. Shoulders, M. D., and Raines, R. T. (2009) *Annu. Rev. Biochem.* **78,** 929–958
35. Weng, H., Mertens, P. R., Gressner, A. M., and Dooley, S. (2007) *J. Hepatol.* **46,** 295–303
36. Yu, H., Pardoll, D., and Jove, R. (2009) *Nat. Rev. Cancer* **9,** 798–809
37. Luppi, F., Losi, M., D'Amico, R., Fabbri, L. M., and Richeldi, L. (2009) *Sarcoidosis Vasc. Diffuse Lung Dis.* **26,** 64–68
38. Azuma, A., Li, Y. J., Abe, S., Usuki, J., Matsuda, K., Henmi, S., Miyauchi, Y., Ueda, K., Izawa, A., Sone, S., Hashimoto, S., and Kudoh, S. (2005) *Am. J. Respir. Cell Mol. Biol.* **32,** 93–98
39. Senft, A. P., Taylor, R. H., Lei, W., Campbell, S. A., Tipper, J. L., Martinez, M. J., Witt, T. L., Clay, C. C., and Harrod, K. S. (2010) *Am. J. Respir. Cell Mol. Biol.* **42,** 404–414
40. Papatheodoridis, G. V., Petraki, K., Cholongitas, E., Kanta, E., Ketikoglou, I., and Manesis, E. K. (2005) *J. Viral. Hepat.* **12,** 199–206
41. Tamai, M., Kawakami, A., Tanaka, F., Miyashita, T., Nakamura, H., Iwanaga, N., Izumi, Y., Arima, K., Aratake, K., Huang, M., Kamachi, M., Ida, H., Origuchi, T., and Eguchi, K. (2006) *J. Lab. Clin. Med.* **147,** 182–190
42. Seo, J. Y., Kim, D. Y., Lee, Y. S., and Ro, J. Y. (2009) *Cytokine* **46,** 51–60
43. Tomita, T., Kido, T., Kurotani, R., Iemura, S., Sterneck, E., Natsume, T., Vinson, C., and Kimura, S. (2008) *J. Biol. Chem.* **283,** 25617–25627
44. Mukherjee, A. B., Kundu, G. C., Mantile-Selvaggi, G., Yuan, C. J., Mandal, A. K., Chattopadhyay, S., Zheng, F., Pattabiraman, N., and Zhang, Z. (1999) *Cell. Mol. Life Sci.* **55,** 771–787
45. Lee, Y. J., and Benveniste, E. N. (1996) *J. Immunol.* **157,** 1559–1568
46. Cheng, M., Nguyen, M. H., Fantuzzi, G., and Koh, T. J. (2008) *Am. J. Physiol. Cell Physiol.* **294,** C1183–C1191
47. Krämer, O. H., and Heinzel, T. (2010) *Mol. Cell Endocrinol.* **315,** 40–48
48. Chiba, Y., Kusakabe, T., and Kimura, S. (2004) *Am. J. Physiol. Lung Cell Mol. Physiol.* **287,** L1193–L1198
49. Chiba, Y., Srisodsai, A., Supavilai, P., and Kimura, S. (2005) *Immunol. Lett.* **97,** 123–129
50. Inoue, K., Wang, X., Saito, J., Tanino, Y., Ishida, T., Iwaki, D., Fujita, T., Kimura, S., and Munakata, M. (2008) *Allergol. Int.* **57,** 57–64

THE JOURNAL OF BIOLOGICAL CHEMISTRY VOL. 286, NO. 20, pp. 17766–17776, May 20, 2011

Identification of Transcription Factor E3 (TFE3) as a Receptor-independent Activator of $G\alpha_{16}$

GENE REGULATION BY NUCLEAR Gα SUBUNIT AND ITS ACTIVATOR[*][S]

Received for publication, January 8, 2011, and in revised form, March 7, 2011 Published, JBC Papers in Press, March 24, 2011, DOI 10.1074/jbc.M111.219816

Motohiko Sato[‡1], Masahiro Hiraoka[‡], Hiroko Suzuki[‡], Yunzhe Bai[‡], Reiko Kurotani[‡], Utako Yokoyama[‡], Satoshi Okumura[‡], Mary J. Cismowski[§], Stephen M. Lanier[¶], and Yoshihiro Ishikawa[‡2]

From the [‡]Cardiovascular Research Institute, Yokohama City University School of Medicine, Fukuura, Yokohama 236-0004, Japan, [§]Center for Cardiovascular and Pulmonary Research, Research Institute at Nationwide Children's Hospital, Columbus, Ohio 43205, and [¶]Department of Pharmacology, Medical University of South Carolina, Charleston, South Carolina 29425

Receptor-independent G-protein regulators provide diverse mechanisms for signal input to G-protein-based signaling systems, revealing unexpected functional roles for G-proteins. As part of a broader effort to identify disease-specific regulators for heterotrimeric G-proteins, we screened for such proteins in cardiac hypertrophy using a yeast-based functional screen of mammalian cDNAs as a discovery platform. We report the identification of three transcription factors belonging to the same family, transcription factor E3 (TFE3), microphthalmia-associated transcription factor, and transcription factor EB, as novel receptor-independent activators of G-protein signaling selective for $G\alpha_{16}$. TFE3 and $G\alpha_{16}$ were both up-regulated in cardiac hypertrophy initiated by transverse aortic constriction. In protein interaction studies *in vitro*, TFE3 formed a complex with $G\alpha_{16}$ but not with $G\alpha_{i3}$ or $G\alpha_s$. Although increased expression of TFE3 in heterologous systems had no influence on receptor-mediated $G\alpha_{16}$ signaling at the plasma membrane, TFE3 actually translocated $G\alpha_{16}$ to the nucleus, leading to the induction of claudin 14 expression, a key component of membrane structure in cardiomyocytes. The induction of claudin 14 was dependent on both the accumulation and activation of $G\alpha_{16}$ by TFE3 in the nucleus. These findings indicate that TFE3 and $G\alpha_{16}$ are up-regulated under pathologic conditions and are involved in a novel mechanism of transcriptional regulation via the relocalization and activation of $G\alpha_{16}$.

Heterotrimeric G-proteins play key roles in transducing cell surface stimuli to intracellular signaling events (1, 2). Activation of G-protein coupled receptors (GPCRs)[3] at the cell surface initiates nucleotide exchange on Gα subunits, leading to a conformational change in $G\alpha\beta\gamma$ and subsequent transduction of signals to various intracellular effector molecules. In addition to the basic components of the G-protein signaling system (*i.e.* GPCRs, heterotrimeric G-proteins, and effector molecules), there is a novel class of regulatory proteins for heterotrimeric G-proteins that directly regulate the activation status of heterotrimeric G-proteins independently of GPCRs (3–10).

Such receptor-independent G-protein regulators are involved in unexpected and important functional roles of heterotrimeric G-proteins in multiple cellular events. For example, LGN (activator of G-protein signaling 5 (AGS5)) and AGS3 are involved in the regulation of mitotic spindle dynamics and cell division (11–14). The GTPase-activating protein RGS14 also translocates between the nucleus and the cytoplasm and is associated with centrosomes influencing mitosis (15). Another RGS protein, RGS7, interacts with $G\beta_5$ and migrates into the nucleus as an RGS7-$G\beta_5$ complex (16). Furthermore, signal alteration by G-protein and their various types of regulators is involved in adaptation of cells to maintain homeostasis under pathologic conditions (17–21). In fact, the expression of such regulatory proteins is altered with the development of cardiac hypertrophy in hypertension or in response to pressure overload stress (22, 23).

As part of a broader approach to identify adaptation-specific regulatory proteins for heterotrimeric G-proteins, we previously identified AGS8 from a cDNA library of rat hearts subjected to repetitive transient ischemia (18). AGS8 was up-regulated in cardiomyocytes in response to transient hypoxia and regulated $G\beta\gamma$ signaling. Indeed, AGS8 played a key role in apoptosis of cardiomyocytes induced by hypoxic stress via $G\beta\gamma$ and the channel protein connexin 43 (24). These findings prompted us to investigate the presence of putative AGS proteins in other models of cardiovascular diseases.

We first screened for regulatory proteins for heterotrimeric G-proteins involved in the development of cardiac

* This work was supported, in whole or in part, by National Institutes of Health Grants NS24821 and DA025896 (both to S. M. L.). This work was also supported by Grants-in-aid for Scientific Research (C) 18599006 and 20590212, the Yokohama Foundation for Advancement of Medical Science, and Strategic Research Project Grants K18017 and K19021 from Yokohama City University, Japan (all to M. S.) and by grants from the Ministry of Health Labor and Welfare; Ministry of Education, Culture, Sports, Science and Technology of Japan; Takeda Science Foundation; Cosmetology Research Foundation; and Kitsuen Research Foundation (all to Y. I.).

[S] The on-line version of this article (available at http://www.jbc.org) contains supplemental Figs. 1 and 2 and Text 1–3.

[1] Supported by the Takeda Science Foundation, the NOVARTIS Foundation (Japan) for the Promotion of Science, the Mitsubishi Pharma Research Foundation, The Ichiro Kanehara Foundation, and the Mochida Memorial Foundation for Medical and Pharmaceutical Research. To whom correspondence may be addressed: Cardiovascular Research Inst., Yokohama City University School of Medicine, 3-9 Fukuura, Kanazawa-Ku, Yokohama 236-0004, Japan. Fax: 81-45-788-1470; E-mail: motosato@yokohama-cu.ac.jp.

[2] To whom correspondence may be addressed. E-mail: yishikaw@med.yokohama-cu.ac.jp.

[3] The abbreviations used are: GPCR, G-protein coupled receptor; TFE, transcription factor E; MITF, microphthalmia-associated transcription factor; TFEB, transcription factor EB; AGS, activators of G-protein signaling; RGS, regulator of G protein signaling; TAC, transverse aortic constriction; PLC, phospholipase C.

hypertrophy. Cardiac hypertrophy is a gateway to cardiac dysfunction and acts as an independent risk factor for cardiovascular events. GPCR-mediated signaling pathways, in particular those involving β-adrenergic or angiotensin II receptors, influence gene expression involved in cardiac hypertrophy. Overexpression of $G\alpha_s$ or $G\alpha_q$ in the mouse heart actually results in the development of cardiac hypertrophy and dysfunction.

We report the identification of three $G\alpha_{16}$-selective AGS proteins using a yeast-based discovery platform for receptor-independent activators of G-protein signaling to screen cDNA libraries from mouse models of cardiac hypertrophy induced by transverse aortic constriction (TAC) or continuous infusion of the β-adrenergic agonist isoproterenol. Of importance, the three new AGS proteins are microphthalmia-associated transcription factor (MITF)/TFE transcription factors. Although increased expression of TFE3 in heterologous systems had no influence on receptor-mediated $G\alpha_{16}$ signaling at the plasma membrane, TFE3 actually translocated $G\alpha_{16}$ to the nucleus, leading to the induction of claudin 14, a key component of membrane structure in cardiomyocytes. These findings indicate that $G\alpha_{16}$-selective AGS proteins are up-regulated under pathologic conditions and are involved in a novel mechanism of transcriptional regulation via the relocalization and activation of $G\alpha_{16}$.

EXPERIMENTAL PROCEDURES

Materials

Anti-$G\alpha_{i3}$, anti-$G\alpha_s$, and anti-phospholipase C (PLC)-β2 antibodies and anti-β_2-adrenergic receptor were purchased from Santa Cruz Biotechnology. IGEPAL CA-630 and anti-β-actin antibody were obtained from Sigma. Anti-$G\alpha_{16}$ and anti-claudin 14 antibodies were purchased from Medical and Biological Laboratories, Co., Ltd. (Nagoya, Japan) and Abcam, respectively. Anti-Xpress antibody and Lipofectamine 2000 reagent were obtained from Invitrogen. pcDNA3.1::$G\alpha_{16}$ and pcDNA3.1::$G\alpha_{16}$Q212L were obtained from the Missouri S&T cDNA Resource Center. $G\alpha_{16}$G211A was generated by site-direct mutagenesis (PrimeSTAR Mutagenesis Basal kit, Takara, Otsu, Japan). Full-length mouse TFE3, human transcription factor EB (TFEB), and mouse MITF were subcloned into the pYES2 vector (Invitrogen) or pcDNAHis vector (Invitrogen) from cDNA clones (Open Biosystems) (TFE3, MMM1013-98478992; TFEB, MHS1010-7508073; MITF, EMM1002-97035453).

Animal Models

All animal experiments were performed according to procedures approved by the Institutional Animal Care and Use Committee at Yokohama City University.

TAC—Constriction of the transverse thoracic aorta was performed on 14 male mice (C57BL/6; age, 14–17 weeks; 24–29 g; Charles River Laboratories, Gilroy, CA) as described previously (25). In brief, mice were anesthetized, intubated, and placed on a respirator. The transverse aorta was visualized following midline sternotomy. A 5-0 nylon suture was placed around the aorta distal to the brachiocephalic artery. The suture was tightened around a blunt 27-gauge needle placed adjacent to the aorta to produce −70% constriction. The needle was then removed, and the chest and overlying skin were closed. Six age-matched animals underwent the same surgical procedure but without TAC (sham). Seven days after surgery, the mice were sacrificed for tissue extraction. The left ventricles were quickly separated, frozen in liquid nitrogen, and stored at −70 °C until use.

Cardiac Hypertrophy and Tachycardia—Nineteen male mice (C57BL/6; age, 16–19 weeks; 25–30 g; Charles River Laboratories) were anesthetized, and an osmotic minipump (model 2002, ALZET Osmotic Pumps, Cupertino, CA) was implanted subcutaneously (18). After 7 days of continuous infusion of isoproterenol (60 μg/g of body weight/day), mice were anesthetized, and the hearts were rapidly excised. The left ventricles were rapidly frozen in liquid nitrogen and stored at −70 °C until use.

Generation of cDNA Libraries and Functional Screen in Saccharomyces cerevisiae

mRNA isolated from the left ventricle in the TAC or tachycardia models was used to synthesize cDNAs using a cDNA Synthesis kit (Takara); cDNAs were cloned into the pYES2 yeast expression vector. The cDNA library from the TAC model contained 1.1×10^6 cfu with an average insert size of 1.5 kb, and the library from tachycardia model contained 2.8×10^6 cfu with an average insert size of 1.2 kb. Functional screens and growth assays in the modified strains of *S. cerevisiae* were conducted as described previously (26–28).

Quantitative Polymerase Chain Reaction (PCR)

RNA isolation, cDNA synthesis, and real time PCR analysis were performed as described previously (24). The primers for RT-PCR were as follows: mouse MITF: forward, 5′-ACTTTCCCTTATCCCATCCACC-3′; reverse, 5′-TGAGATCCAGAGTTGTCGTACA-3′; mouse TFE3: forward, 5′-TGCGTCAGCAGCTTATGAGG-3′; reverse, 5′-AGACACGCCAATCACAGAGAT-3′; mouse TFEB: forward, 5′-CCACCCCAGCCATCAACAC-3′; reverse, 5′-CAGACAGATACTCCCGAACCTT-3′; mouse GNA15: forward, 5′-CGCCAGAATCGACCAGGAG-3′; reverse, 5′-GTAGCCCACACCGTGAATGA-3′; mouse claudin 14: forward, 5′-GCATGGTGGGAACGCTCAT-3′; reverse, 5′-CCACAGTCCCTTCAGGTAGGA-3′; human claudin 14: forward, 5′-CAAACACCGCACCTGCCTA-3′; reverse, 5′-CACGTAGTCGTTCAGCCTGT-3′; rat GNA15: forward, 5′-CAGGAGAACCGTATGAAGGAGAGTC-3′; reverse, 5′-CAGGATGTCTGTCTTGTTGAGGAAG-3′; rat TFE3: forward, 5′-TGTTCGTGCTGTTGGAAGAGC-3′; reverse, 5′-GGGATAGAGGCTGGCTTTTGAG-3′; rat claudin 14: forward, 5′-TCATCACTACTATCCTGCCGCAC-3′; reverse, 5′-ACACACTCCATCCACAGTCCCTTC-3′; and 18 S: forward, 5′-GTAACCCGTTGAACCCCATT-3′; reverse, 5′-CCATCCAATCGGTAGTAGCG-3′. All PCRs were performed in duplicate or triplicate at 95 °C for 2 min followed by 40 cycles at 95 °C for 30 s and 60 or 62 °C for 45 s. The cycle threshold values corresponding to the PCR cycle number at which fluorescence emission in real time reaches a threshold above the base-line emission were determined. 18 S ribosomal

RNA was used as a control for the amount of target mRNA in each sample.

Generation of Glutathione S-Transferase (GST) Fusion Protein, Protein Interaction Assays, and Immunoblotting

The coding sequence of TFE3 (amino acids Leu^{40}–Ser^{572}; cDNA1-8) was amplified by PCR and fused in-frame to GST in the pGEX-6T vector (Amersham Biosciences). The GST-TFE3 fusion protein was expressed in bacteria (*Escherichia coli* BL21; Amersham Biosciences) and purified on a glutathione affinity matrix. The GST fusion protein was eluted from the resin, and glutathione was removed by desalting to allow a solution-phase interaction assay (17). Protein interaction assays and immunoblotting were performed as described previously (17, 29).

Cell Culture and Transfection

COS7 or HEK293 cells were cultured and transfected as described previously (17). In brief, cells were suspended at 0.5–1.0 × 10^5 cells/ml, and 1.0 (12-well plate), 2.0 (35-mm dish), or 10 ml (100-mm dish) was plated. After 18 h, cells were transfected with 2 (12-well plate), 4–5 (35-mm dish), or 12 μg (100-mm dish) of cDNA with Lipofectamine 2000 (Invitrogen) as recommended by the manufacturer. For each experiment, transfection efficiency was monitored by pEGFP vector transfection to generate a fluorescent signal and immunoblotting. The transfection efficiency was 60–80%. Cell lysis and fractionation were performed as described previously (17, 30).

Transfection of Small Interfering RNA (siRNA) to Cultured Cardiomyocytes

Double strand siRNA oligonucleotides to rat *GNA15* ($G\alpha_{16}$; NCBI Reference Sequence NM_053542) and *TFE3* (NCBI Reference Sequence XM_228760) were synthesized (Stealth siRNA, Invitrogen) as follows: GNA15 siRNA: sense, 5′-CCAUGCAGGCCAUGAUUGAAGCAAU-3′; TFE3: sense, 5′-CAGAAGAAAGACAAUCACAACCUAA-3′. The conditions and duplex eliciting the most effective reduction in GNA15 and TFE3 were determined in a series of preliminary experiments. Cardiomyocytes were prepared from the hearts of 1–3-day-old Wistar rats as described previously (24). Approximately 24 h after preparation, neonatal cardiomyocytes at 4.0 × 10^5 cells in 35-mm plates were transfected with siRNA using Lipofectamine 2000 according to the manufacturer's instructions. Briefly, GNA15siRNA and TFE3siRNA individually in 50 μl of Opti-MEM I medium (Invitrogen) and 2.5 μl of Lipofectamine 2000 in 50 μl of Opti-MEM I medium were mixed, and then the mixture was added to cardiomyocytes. The final concentrations of GNA15siRNA and TFE3siRNA were 50 and 100 nM, respectively. The transfection efficiency of FITC-labeled oligonucleotide was 70–80%. The decrease of mRNA of GNA15 or TFE3 was confirmed by real time PCR following transfection of siRNAs.

Immunoprecipitation

Cell lysates were prepared in 250–500 μl of immunoprecipitation buffer (50 mM Tris, pH 7.4, 70 mM NaCl, 5 mM EDTA, 1% IGEPAL CA-630 (Sigma), and a protease inhibitor mixture (Complete Mini, Roche Applied Science)). The lysates were incubated with 1.0–3.5 μg of antibody for 18 h after preclearing with 25 μl of 50% Sepharose-G for 1 h at 4 °C. The samples were incubated with 25 μl of 50% Sepharose-G for 1 h at 4 °C, and the pellets were washed three times with immunoprecipitation buffer. Proteins were eluted in 30 μl of 2× Laemmli buffer and resolved by SDS-PAGE (24).

Measurements of Inositol Phosphates

COS7 cells were seeded in 12-well plates at 0.5–1.0 × 10^5 cell/well. Next, 40 h after transfection, the cells were washed three times with phosphate-buffered saline (PBS) and incubated with serum-free Dulbecco's modified Eagle's medium for 4 h. The amount of cellular inositol monophosphate was determined by IP-One ELISA (Cisbio) according to the manufacturer's protocol.

Immunocytochemistry

Tissue Sections—Mouse heart was fixed in 4% paraformaldehyde and embedded in paraffin. Sections (4 μm thick) were prepared after being deparaffinized with xylene and graded ethanol. Sections were incubated in 0.3% H_2O_2 in methanol for 30 min to inactivate endogenous peroxidases and then rinsed three times for 5 min each with PBS. Tissues were incubated in citrate buffer (pH 6.0) at 100 °C for 10 min. Tissues were blocked in 5% skim milk for 30 min at room temperature and then incubated overnight with goat anti-claudin 14 (ab19035, Abcam; 1:100) antibodies at 4 °C in a humidified chamber. After washing three times for 5 min each in PBS, tissues were processed by the avidin-biotin complex method using a commercially available kit (Vector Laboratories, Burlingame, CA) according to the manufacturer's instructions. Immunocomplexes were visualized with 3,3′-diaminobenzidine tetrahydrochloride (DAB) (Dako, Glostrup, Denmark) or with the Liquid DAB-Black Substrate kit (Zymed Laboratories Inc., San Francisco, CA).

Cultured Cells—Cells were seeded on 24 × 24-mm polylysine-coated coverslips. Cells were fixed with PBS containing 4% paraformaldehyde and 4% sucrose for 15 min and then incubated with 0.2% Triton X-100 in PBS for 5 min. After three washes with PBS, cells were incubated with 5% normal donkey serum in PBS for 1 h. Cells were incubated with primary antibodies for 18 h at 4 °C followed by incubation for 1 h with secondary antibody (goat anti-mouse Alexa Fluor 488 or goat anti-rabbit Alexa Fluor 594, highly cross-absorbed; Molecular Probes) diluted to 1:2000 in PBS. All antibody dilutions were centrifuged at 12,000 × *g* for 15 min prior to use. In some cases, cells were incubated with 1 μg/ml 4′,6′-diamidino-2-phenylindole, dihydrochloride (DAPI) (Molecular Probes) in PBS for 5 min after incubation with secondary antibodies. Slides were then mounted with glass coverslips with ProLong Gold antifade reagent (Invitrogen). Images were analyzed by deconvolution microscopy (TE2000-E, Nikon, Tokyo, Japan). Obtained images were deconvoluted using NIS-Elements 3.0 software (Nikon) with a "no neighbors" deconvolution algorithm. All images were obtained from approximately the middle plane of the cells.

TABLE 1

AGS cDNAs isolated from cardiac hypertrophy model of mouse

AGSs are numbered according to the order in which they were isolated from a functional screen in yeast. GPR, G-protein-regulatory motif. The number of transformants screened for each cDNA library of the heart is as follows: transverse aortic constriction, 1.6×10^7; isoproterenol infusion, 2.0×10^7.

Gene in database	AGS	Cardiac dysfunction model used to generate cDNA libraries for functional screen[a]	
		Transverse aortic constriction	Isoproterenol infusion
Dynlt1b (the entire coding sequence)	AGS2	+	−
GPSM1 (C-terminal 178 amino acids with 3 GPR motifs)	AGS3	+	−
RGS12 (C-terminal 206 amino acids with GPR motif)	AGS6	+	+
TFE3 (C-terminal 533 amino acids)	AGS11	+	+
TFEB (C-terminal 320 amino acids)	AGS12	−	+
MITF (C-terminal 304 amino acids)	AGS13	+	+

[a] cDNA libraries were screened in yeast strains CY1141 ($G\alpha_{i3}$), CY8342 ($G\alpha_s$), and CY9603 ($G\alpha_{16}$).

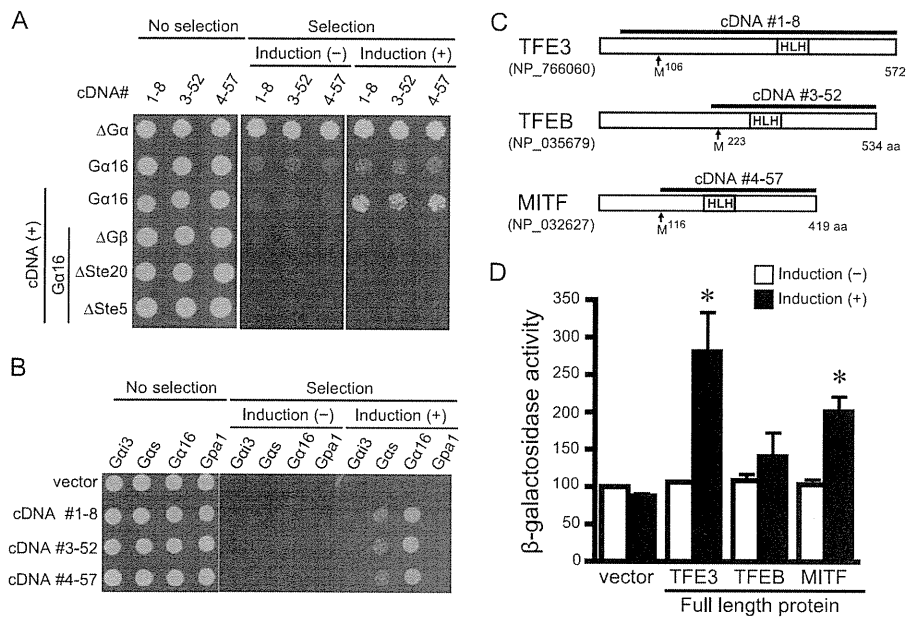

FIGURE 1. **Bioactivity and diagram of AGSs isolated from mouse hypertrophic heart.** In *A* and *B*, data are presented in three panels to illustrate the viability of the transformed yeast and the galactose-dependent growth under the selective pressure of exclusion of histidine from the medium. Galactose promotes the expression of each cDNA in the pYES2-containing *GAL1* promoter. About 2000 cells were suspended in H_2O and spotted on medium with glucose plus histidine (*left*; no selection), glucose minus histidine (*center*; selection without induction), or galactose plus histidine (*right*; selection plus induction). *A*, epistasis analysis of isolated clones. Transformants in a yeast strain expressing human $G\alpha_{16}$ (Gpa1(1–41)) and yeast lacking Gα, Gβ, or downstream signaling molecules (Δ*Gα*, yeast lacking Gα; Δ*Gβ*, yeast lacking Gβ; Δ*Ste20*, yeast lacking p21-activated kinase; Δ*Ste5*, yeast lacking the kinase scaffold protein). *B*, effect of isolated cDNAs in yeast expressing various types of Gα. *C*, schematic diagram of the sequences of TFE3, TFEB, and MITF in mouse. The *line above* the sequence refers to cDNA isolated by the yeast-based functional screen. *HLH*, helix-loop-helix. *D*, bioactivity of full-length TFE3, TFEB, and MITF. The full-length clones were transformed into yeast expressing $G\alpha_{16}$. The magnitude of activation of G-protein signaling pathway was monitored by β-galactosidase activity. Data are presented as the mean S.E. of five experiments with duplicate determinations. *, $p < 0.05$ *versus* non-induction group.

Miscellaneous Procedures and Statistical Analysis

Immunoblotting and data analysis were performed as described previously (18, 24). The luminescence images captured with an image analyzer (LAS-3000, Fujifilm, Tokyo, Japan) were quantified using Image Gauge 3.4 (Fujifilm). Data are expressed as mean ± S.E. from independent experiments as described in the figure legends. Statistical analyses were performed using the unpaired *t* test, F-test, and one-way analysis of variance followed by Tukey's multiple comparison post hoc test. All statistical analyses were performed with Prism 4 (GraphPad Software).

RESULTS

Identification of Activators of G-protein Signaling from Hypertrophied Hearts—We utilized an expression cloning system in *S. cerevisiae* to identify receptor-independent activators of G-protein signaling involved in the development of cardiac hypertrophy (18, 26). The yeast strains used in this screen system lacked the pheromone receptor but expressed mammalian Gα ($G\alpha_{i3}$, $G\alpha_s$, or $G\alpha_{16}$) in place of the yeast Gα subunit and provided a readout of growth upon activation of the G-protein-regulated pheromone signaling pathway. cDNA libraries from the left ventricle of the hypertrophy models were constructed in a galactose-inducible vector and introduced into these yeast strains. Functional screening for receptor-independent AGS proteins was then facilitated by selection of colonies growing in a galactose-specific manner.

We used two models of cardiac hypertrophy: the TAC-induced pressure overload model and the isoproterenol-induced tachycardiac hypertrophic model (supplemental Fig. 1). cDNA libraries from each model were introduced into the yeast strains expressing mammalian $G\alpha_{i3}$, $G\alpha_s$, or $G\alpha_{16}$ (Table 1). Twenty-

nine cDNA clones encoding six distinct proteins were isolated from the two cDNA libraries ($G\alpha_s$ strain, 0; $G\alpha_{i3}$ strain, 20; $G\alpha_{16}$ strain, 9). Each clone was retransformed into yeast to confirm plasmid-dependent growth, and then epistasis analysis was performed to identify the site of action within the pheromone pathway. Epistasis analysis demonstrated that six of these cDNA clones required G-protein to activate the growth-linked G-protein pathway, and thus these clones satisfied the definition of AGS (3, 27) (Table 1 and Fig. 1*A*).

Three clones isolated from yeast expressing $G\alpha_{i3}$ encoded the previously characterized proteins AGS2 (*Dynlt1b*, NCBI Reference Sequence NM_033368), AGS3 (*GPSM1*, NCBI Reference Sequence NM_700459), and AGS6 (*RGS12*, NCBI Reference Sequence NM_001156984). The cDNAs encoding AGS3 and AGS6 contained the G-protein-regulatory motif(s) that stabilizes the GDP-bound conformation of $G\alpha_i$, transducin, and $G\alpha_o$. An additional three cDNAs (1-8, 3-52, and 4-57) were isolated from yeast expressing $G\alpha_{16}$. These three cDNAs exhibited bioactivity in yeast strains expressing $G\alpha_{16}$ but not in yeast expressing $G\alpha_{i3}$, $G\alpha_s$, or Gpa1 (yeast $G\alpha$), indicating $G\alpha$ selectivity (Fig. 1*B* and supplemental Text 1). We therefore focused on these $G\alpha_{16}$-specific AGS cDNAs.

$G\alpha_{16}$-specific AGS Proteins—Sequence analysis of the $G\alpha_{16}$-specific cDNAs indicated that all encoded MITF/TFE transcription factors (31–33). cDNA1-8 encoded the C-terminal 533 amino acids of TFE3 (NCBI Reference Sequence NP_766060), cDNA3-52 encoded the C-terminal 320 amino acids of TFEB (NCBI Reference Sequence NP_035679), and cDNA4-57 encoded the C-terminal 304 amino acids of MITF (NCBI Reference Sequence NP_032627) (Fig. 1*C*). In accordance with the numbering of previously discovered AGS proteins (18), cDNA1-8, cDNA3-52, and cDNA4-57 were termed AGS11, AGS12, and AGS13, respectively (Table 1).

Full-length TFE3, TFEB, and MITF were cloned into a yeast expression vector, and the bioactivity for the G-protein signaling pathway was determined by β-galactosidase reporter assays (Fig. 1*D*). Full-length TFE3 and MITF, but not TFEB, activated the G-protein pathway in $G\alpha_{16}$-expressing cells. Full-length TFE3, MITF, and TFEB did not activate growth of yeast expressing $G\alpha_s$ (supplemental Text 2). Immunoblot analysis indicated that the full-length proteins were expressed at the

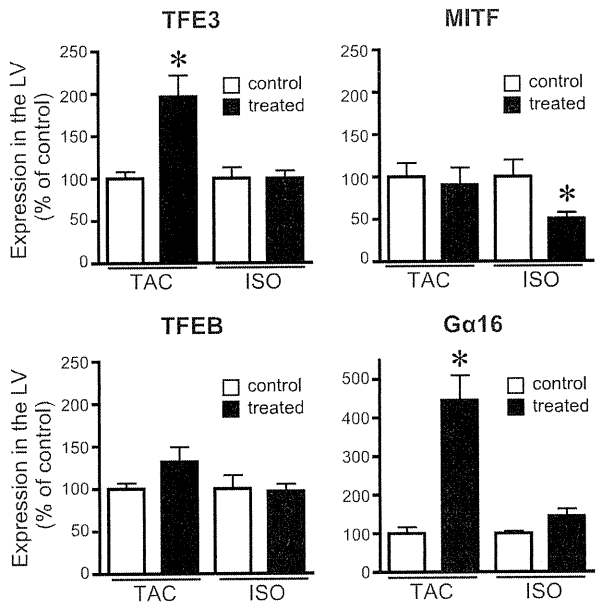

FIGURE 2. **Expression of MITF/TFE transcription factors and $G\alpha_{16}$ in mouse cardiac hypertrophy model.** The expression of mRNA of each gene was analyzed by real time PCR as described under "Experimental Procedures." *Control* refers to the sham-operated or saline-infused mouse. Data are expressed as the -fold change in level compared with the control group. *ISO*, continuous infusion of isoproterenol; *LV*, left ventricle. Data are presented as the mean ± S.E. of five experiments with duplicate determinations. *, $p < 0.05$ *versus* control group.

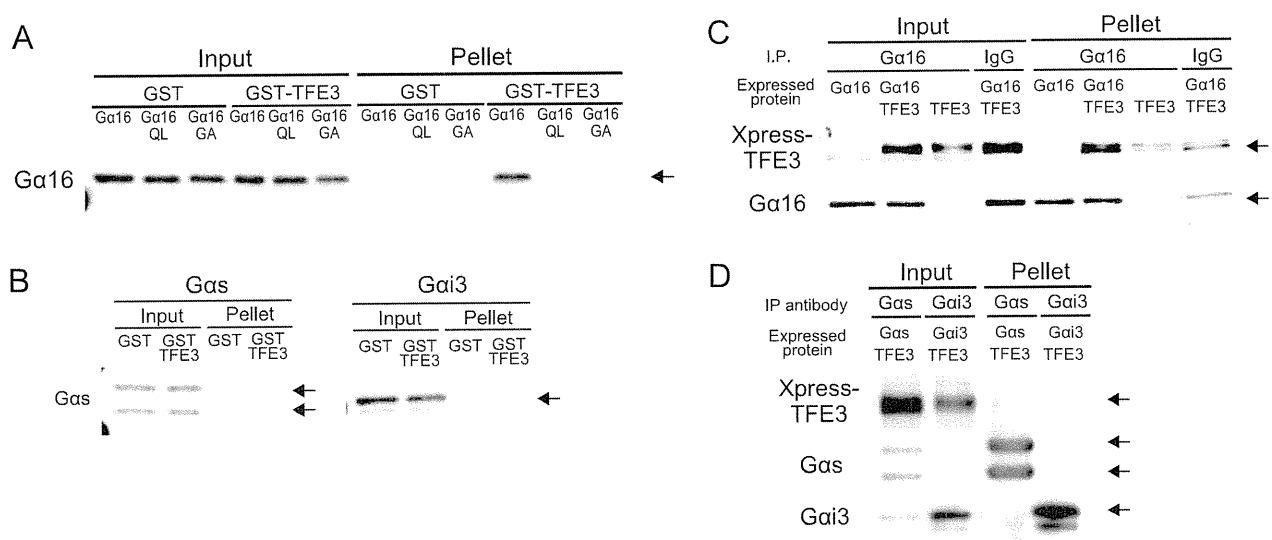

FIGURE 3. **Interaction of TFE3 with $G\alpha_{16}$ *in vitro* and in cell.** *A* and *B*, GST pulldown assay of TFE3 with COS7 lysate expressing various Gα subunits. The C-terminal 533-amino acid fragment of TFE3 was expressed as a GST fusion protein (GST-TFE3). GST-TFE3 (300 nM) was incubated with 1 mg of cell lysate in a total volume of 500 μl at 4 °C. Lysates of COS7 cells were prepared as described under "Experimental Procedures" following transfection of 10 μg of the Gα subunit in pcDNA3. *C* and *D*, COS7 cells in a 100-mm dish were transfected with a combination of pcDNA3, pcDNA3::$G\alpha_{16}$ (5 μg/dish), and pcDNA3.1-His::TFE3 (5 μg/dish). The amount of DNA transfected was adjusted to 10 μg/well with the pcDNA3 vector. The preparation of a whole-cell lysate including the nuclear fraction and immunoprecipitation (*IP*) were performed as described under "Experimental Procedures." The Gα subunit was immunoprecipitated with a specific antibody for each Gα subunit. *QL*, $G\alpha_{16}$Q212L; *GA*, $G\alpha_{16}$G211A.

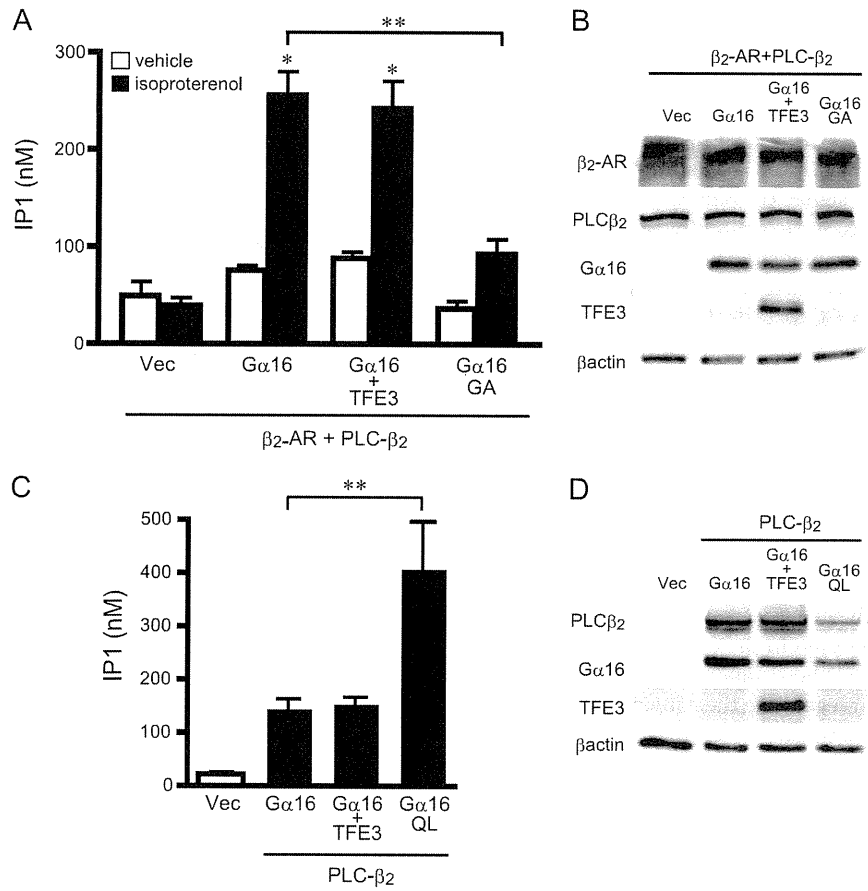

FIGURE 4. **Effect of TFE3 on activation of phospholipase C-β2.** *A*, effect of TFE3 on the generation of inositol phosphate (*IP1*) following receptor stimulation. COS7 cells were transfected in 12-well plates with control vectors (*Vec*) or cDNAs as indicated (0.4 μg of pcDNA::PLC-β2, 0.5 μg of pcDNA::TFE3, 0.5 μg of pcDNA::$G\alpha_{16}$, and 0.6 μg of pEGFP::β_2-adrenergic receptor (*AR*)). The amount of transfected DNA was adjusted to 2 μg/well with the pcDNA vector. Cells were stimulated with 10 μM isoproterenol for 30 min and assayed immediately. Data are expressed as the mean ± S.E. of five experiments with duplicate determinations. *B*, expression of transfected proteins of *A*. The expression of each protein was determined by immunoblotting of 10 μg of whole-cell lysates. *C*, effect of TFE3 on the generation of inositol phosphate. COS7 cells were transfected in 12-well plates with control vectors or cDNAs as indicated (0.5 μg of pcDNA::PLC-β2, 0.75 μg of pcDNA::TFE3, and 0.75 μg of pcDNA::$G\alpha_{16}$). The amount of transfected DNA was adjusted to 2 μg/well with the pcDNA vector. Data are expressed as the mean ± S.E. of five experiments with duplicate determinations. *D*, expression of transfected cDNA of *C*. The expression of each protein was determined by immunoblotting of 10 μg of whole-cell lysates. *, $p < 0.05$ *versus* control group; **, $p < 0.05$ between two groups. *QL*, $G\alpha_{16}$Q212L; *GA*, $G\alpha_{16}$G211A.

expected size and that their expression did not alter the levels of $G\alpha_{16}$. These findings suggest that TFE3, MITF, and TFEB are transcription factors that act as receptor-independent G-protein activators. AGSs with various functions have been identified; however, no transcription factors have previously been described as AGS proteins.

Expression of TFE3, TFEB, and MITF in Cardiac Hypertrophy Models—It was reported previously that the expression level of MITF was associated with development of cardiac hypertrophy in mouse (34). We sought to determine whether the three $G\alpha_{16}$-specific AGS proteins were up-regulated in cardiac hypertrophy or were constitutively expressed in the myocardium. RNA expression of TFE3, MITF, TFEB, and the target $G\alpha_{16}$ subunit was determined in the hypertrophied myocardium (Fig. 2). TFE3 mRNA expression was up-regulated in the left ventricle in the TAC model but not in the isoproterenol model. MITF was unchanged in the TAC model but reduced in the isoproterenol model. TFEB did not show any significant changes of expression in either model. Notably, $G\alpha_{16}$ mRNA expression was also increased in the TAC model in which TFE3 was up-regulated. As TFE3 and $G\alpha_{16}$ were both significantly up-regulated in the TAC model, we focused on the characterization of TFE3.

Formation of TFE3-$G\alpha_{16}$ Complex in Cells—The above findings suggested that TFE3 plays an important role via $G\alpha_{16}$ in the development of cardiac hypertrophy. We thus examined whether TFE3 indeed was able to form a complex with $G\alpha_{16}$. As a first approach, the interaction of GST-tagged TFE3 (GST-TFE3) with $G\alpha_{16}$ was examined *in vitro*. GST-TFE3 successfully pulled down transfected $G\alpha_{16}$ from cell lysates. However, neither a constitutively active mutant of $G\alpha_{16}$ ($G\alpha_{16}$Q212L) nor an inactive mutant of $G\alpha_{16}$ ($G\alpha_{16}$G211A) was pulled down, suggesting that the interaction of $G\alpha_{16}$ and TFE3 was dependent upon the conformation of $G\alpha_{16}$ and regulated by guanine nucleotide binding (Fig. 3*A*) (35, 36). In contrast, GST-TFE3 did not pull down transfected $G\alpha_s$ or $G\alpha_{i3}$ from cell lysates (Fig. 3*B*). We also examined whether TFE3 interacted with $G\alpha_{16}$ in mammalian cells. Expressed TFE3 was co-immunoprecipitated with $G\alpha_{16}$ from COS7 cell lysates, suggesting that TFE3 and $G\alpha_{16}$ formed a stable complex

within these cells (Fig. 3*C*). In contrast, TFE3 did not co-immunoprecipitate with $G\alpha_s$ or $G\alpha_{i3}$ (Fig. 3*D*). We next examined the role of this interaction in $G\alpha_{16}$-mediated signaling events.

TFE3 Is Not Involved in Receptor-mediated $G\alpha_{16}$ Signaling—$G\alpha_{16}$ is coupled to multiple GPCRs including β_2-adrenergic receptors mediating signal transfer to the effector molecule PLC-β (37, 38). Thus, we examined whether TFE3 regulated β_2-adrenergic receptor-mediated PLC-β2 activation as a representative of $G\alpha_{16}$-mediated signaling (39). In a transient expression system in COS7 cells, $G\alpha_{16}$ activated PLC-β2 following β_2-adrenergic receptor stimulation as determined by inositol monophosphate production (Fig. 4). The magnitude of PLC-β2 activation was reduced in the presence of an inactive $G\alpha_{16}$ mutant ($G\alpha_{16}$G211A), indicating that PLC-β2 activation was mediated by $G\alpha_{16}$ (Fig. 4, *A* and *B*). However, TFE3 overexpression did not alter this receptor-mediated $G\alpha_{16}$ signaling. We also examined the effect of TFE3 overexpression on the basal activity of PLC-β2/$G\alpha_{16}$ in the absence of receptor stimulation. TFE3 overexpression did not alter PLC-β2 activity, whereas a constitutively active mutant of $G\alpha_{16}$ ($G\alpha_{16}$Q212L) increased the activity even in the absence of receptor stimulation (Fig. 4, *C* and *D*). These data are consistent with a lack of TFE3 involvement in regulating the conventional GPCR-mediated $G\alpha_{16}$ signaling pathway.

TFE3 Induces Accumulation of $G\alpha_{16}$ in Nucleus—The identification of transcription factors as $G\alpha_{16}$-specific AGS proteins suggested that MITF/TFE transcription factors may interact with a subpopulation of $G\alpha_{16}$ distinct from that involved in the conventional G-protein signaling at the plasma membrane. To address this issue, we first examined the subcellular distribution of $G\alpha_{16}$ and TFE3 when each was independently overexpressed in the cell. Overexpressed TFE3 was predominantly found in the nucleus as expected, whereas $G\alpha_{16}$ was found in the plasma membrane and cytoplasm but not in the nucleus (Fig. 5, *arrow*, and supplemental Fig. 2, A, B, and D). However, when $G\alpha_{16}$ and TFE3 were overexpressed together, $G\alpha_{16}$ predominantly accumulated in the nucleus (Fig. 5, *arrow*). This novel nuclear translocation of $G\alpha_{16}$ was not due to $G\alpha_{16}$ activation because the constitutively active mutant of $G\alpha_{16}$ ($G\alpha_{16}$Q212L) was not found in the nucleus when it was overexpressed by itself. These data suggested that $G\alpha_{16}$ forms a complex with TFE3 and translocates to the nucleus. Nuclear accumulation of G-protein by TFE3 was not observed for $G\alpha_{i3}$ or $G\alpha_s$.

Up-regulation of Claudin 14 mRNA by TFE3-$G\alpha_{16}$ Complex—The co-localization of TFE3 and $G\alpha_{16}$ suggested an involvement of a nuclear TFE3-$G\alpha_{16}$ complex in regulating the expression of particular genes. To address this issue, genes regulated by TFE3 and $G\alpha_{16}$ were screened by microarray analysis of mRNA of HEK293 cells transfected with TFE3 and/or $G\alpha_{16}$. In the screening of more than 40,000 human genes, we found that claudin 14 mRNA was highly up-regulated by the simultaneous transfection of TFE3 and $G\alpha_{16}$. Parallel experiments indicated that the co-overexpression of TFE3 and $G\alpha_{16}$ in HEK293 cells increased claudin 14 mRNA by 133-fold, whereas independent overexpression of TFE3 (8.3-fold) or $G\alpha_{16}$ (1.0-fold) had minimal effect on the induction of claudin 14 (Fig. 6*A*). The induction of claudin 14 was significantly decreased in the presence of the inactive mutant of $G\alpha_{16}$ ($G\alpha_{16}$G211A) compared with wild type $G\alpha_{16}$, suggesting that $G\alpha_{16}$ activation was also required for the induction of this gene.

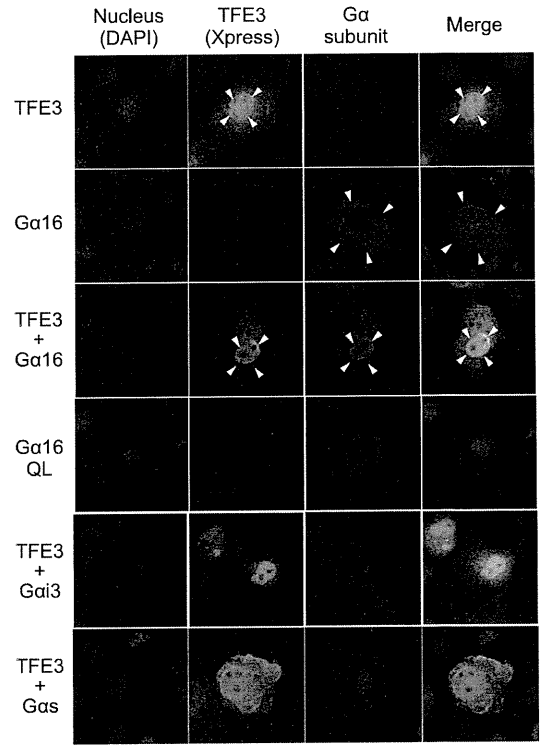

FIGURE 5. **Localization of expressed Gα subunits and TFE3 in COS7 cells.** COS7 cells were transfected in a 35-mm dish with 2.0 μg of Gα subunits in pcDNA3 and/or 2.0 μg of pcDNA3.1-His::TFE3. The amount of transfected DNA was adjusted to 4 μg/well with the pcDNA3 vector. The Gα subunit and TFE3 were determined using a specific antibody for each Gα (*red*) or Xpress antibody (*green*), respectively. *QL*, $G\alpha_{16}$Q212L.

Requirement of $G\alpha_{16}$ Activation for Gene Induction by TFE3—The requirement of $G\alpha_{16}$ activation for this gene induction was further characterized utilizing a truncated mutant of TFE3 (delTFE3), which showed less bioactivity for $G\alpha_{16}$ activation in the yeast system. Analysis of the amino acid sequences of the MITF/TFE family indicated that the C-terminal 27 acids were conserved among the $G\alpha_{16}$-selective AGS proteins (Fig. 6*B*, *upper panel*). Deletion of the C-terminal 27 amino acids resulted in the loss of bioactivity of TFE3 and MITF for G-protein activation (Fig. 6*B*, *left middle panel*, and supplemental Text 3). Despite the loss of bioactivity for $G\alpha_{16}$ activation, delTFE3 was still able to form a complex with $G\alpha_{16}$ and induce the translocation of $G\alpha_{16}$ to the nucleus (Fig. 6*B*, *left lower* and *right panels*, and supplemental Fig. 2, C and D). Thus, nuclear translocation by itself did not require $G\alpha_{16}$ activation as long as TFE3 and $G\alpha_{16}$ formed a complex (Fig. 6*A*).

Although the delTFE3-$G\alpha_{16}$ complex was found in the nucleus, the subsequent up-regulation of claudin 14 was blunted, suggesting that $G\alpha_{16}$ activation is critical for this gene induction (Fig. 6*A*). Furthermore, the constitutively active mutant of $G\alpha_{16}$ ($G\alpha_{16}$Q212L), which was not expressed in the nucleus (Fig. 5), failed to induce claudin 14. MITF, which had a similar ability to activate $G\alpha_{16}$ (Fig. 1*D*), failed to induce claudin

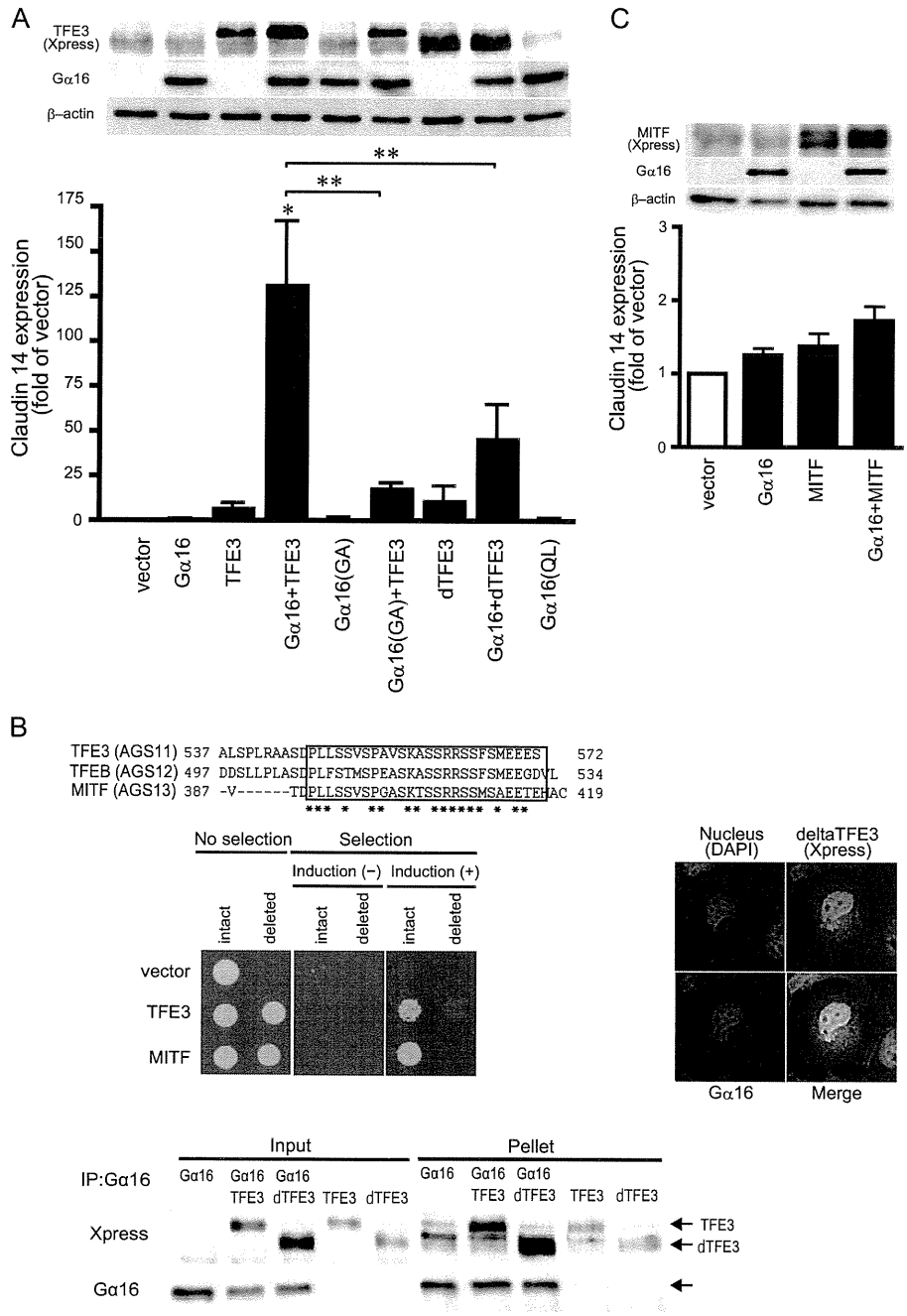

FIGURE 6. **Effect of TFE3 or MITF on expression of claudin 14.** *A*, expression of claudin 14 in transfected HEK293 cells. HEK293 cells were transfected in 6-well plates with a combination of control vectors or cDNAs as indicated (2.0 μg of Gα subunits in pcDNA3 and 2.0 μg of TFE3 or delTFE3 in pcDNA3.1-His). The amount of transfected DNA was adjusted to 4 μg/well with the pcDNA3 vector. The expression of claudin 14 mRNA was analyzed by real time PCR. Data are expressed as the -fold change from the level of claudin 14 expression in control cells transfected with the vector alone. Data are expressed as the mean ± S.E. of five experiments with duplicate determinations. *Upper inset*, expression of proteins determined by immunoblotting (~10 μg of whole-cell lysate). Data are representative of five experiments. *, $p < 0.05$ *versus* control group; **, $p < 0.05$ between two groups. *B*, effect of delTFE3. *Upper panel*, amino acid sequence of C-terminal MITF/TFE transcription factors. The *square* indicates conserved amino acid sequence. *, consensus amino acid. *Middle left panel*, bioactivity of intact or deleted TFE3 in yeast expressing Gα_{16}. The assay was performed as described under "Experimental Procedures." *Middle right panel*, localization of transfected Gα_{16} and TFE3 in COS7 cells. COS7 cells were transfected in a 35-mm dish with 2.0 μg of pcDNA3::Gα_{16} and 2.0 μg of pcDNA3.1-His::TFE3. Gα_{16} and TFE3 were determined using Gα_{16} antibody (*red*) or Xpress antibody (*green*), respectively. *Lower panel*, interaction of Gα_{16} with TFE3 or delTFE3. COS7 cells in a 100-mm dish were transfected with a combination of pcDNA3, pcDNA3::Gα_{16} (5 μg/dish), pcDNA3.1-His::TFE3 (5 μg/dish), and pcDNA3.1-His::delTFE3 (5 μg/dish). The amount of transfected DNA was adjusted to 10 μg/well with the pcDNA3 vector. The preparation of the cell lysate and immunoprecipitation (*IP*) were performed as described under "Experimental Procedures". *C*, effect of MITF on claudin 14 expression in transfected HEK293 cells. HEK293 cells were transfected in 6-well plates with a combination of control vectors or cDNAs as indicated (2.0 μg of pcDNA3::Gα_{16} and 2.0 μg of pcDNA3.1-His::MITF). The amount of transfected DNA was adjusted to 4 μg/well with the pcDNA3 vector. The expression of claudin 14 mRNA was analyzed by real time PCR. Data are expressed as the -fold change in the level of claudin 14 in control cells transfected with the vector alone. Data are expressed as the mean ± S.E. of five experiments with duplicate determinations. *Upper inset*, expression of proteins determined by immunoblotting (~10 μg of whole-cell lysate). Data are representative of five experiments. *QL*, Gα_{16}Q212L; *GA*, Gα_{16}G211A.

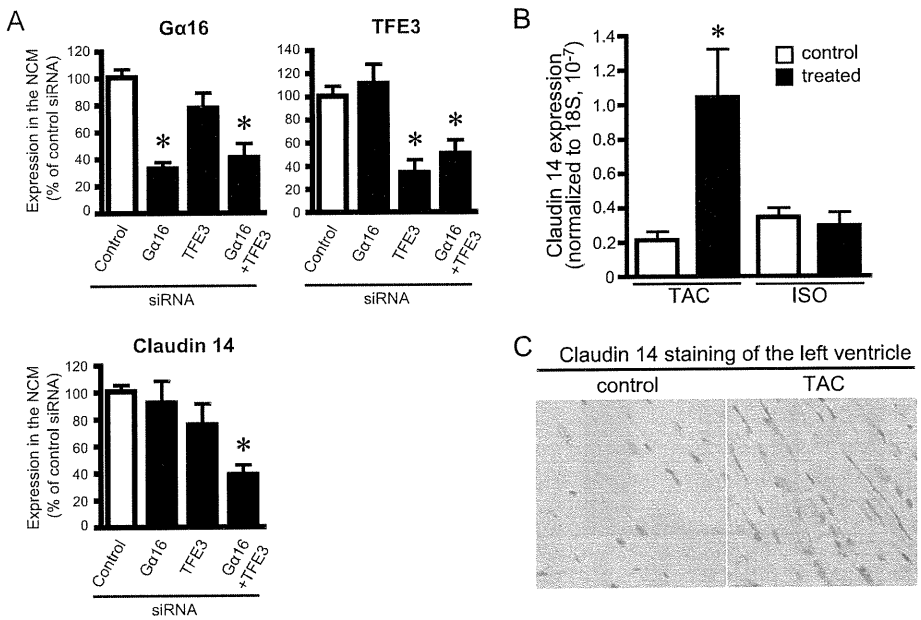

FIGURE 7. **Expression of claudin 14 in cultured cardiomyocytes and hypertrophied heart.** *A*, effect of knockdown of $G\alpha_{16}$ and TFE3 on the level of claudin 14 mRNA in cultured cardiomyocytes. Neonatal cardiomyocytes (*NCM*) were transfected with each siRNA and/or universal control siRNA (Stealth RNAi Negative Control, Invitrogen). Forty-eight hours after transfection, the level of mRNA of $G\alpha_{16}$ (*A*), TFE3 (*B*), and claudin 14 (*C*) were analyzed by real time PCR. Transfection efficiency of siRNA was estimated at 70–80% using FITC-labeled double strand RNA (Block It Fluorescent Oligo, Invitrogen) (*right panel*). *, $p < 0.05$ *versus* negative siRNA. Data are expressed as the mean ± S.E. of seven to eight independent experiments. *B* and *C*, expression of claudin 14 in the mouse cardiac hypertrophy model. *B*, the left ventricular expression of claudin 14 mRNA was analyzed by real time PCR. *Control* refers to the sham-operated or saline-infused mouse. Data are expressed as the -fold change in claudin 14 level from that in control group. Data are expressed as the mean ± S.E. of five experiments with duplicate determinations. *C*, immunohistochemical staining for claudin 14 (1:100; *brown*) of the left ventricle of sham- or TAC-operated mouse. A frozen section (8 μm) of the mouse heart was subjected to immunohistochemical staining as described under "Experimental Procedures". *Blue*, nucleus. *ISO*, continuous infusion of isoproterenol. *, $p < 0.05$ *versus* control group.

14 (Fig. 6*C*). Taken together, the results suggest that in addition to the nuclear translocation of a TFE3-$G\alpha_{16}$ complex activation of $G\alpha_{16}$ in the nucleus was required for the induction of claudin 14.

Regulation of Claudin 14 Expression in Cardiomyocytes—The influence of $G\alpha_{16}$ and TFE3 on the expression of claudin 14 was also examined in neonatal cardiomyocytes following knockdown of $G\alpha_{16}$ and/or TFE3 by siRNA. $G\alpha_{16}$siRNA or TFE3siRNA successfully suppressed the level of target molecules to 33–34% of the level of cardiomyocytes treated with negative control siRNA (Fig. 7*A*). The level of claudin 14 in cardiomyocytes was not influenced by $G\alpha_{16}$siRNA or TFE3siRNA itself when they were separately introduced (Fig. 7*A*, *lower panel*). However, interestingly, the simultaneous knockdown of $G\alpha_{16}$ and TFE3 by siRNAs significantly reduced the claudin 14 mRNA (38.9 ± 7.4%, $p < 0.05$ *versus* control siRNA), indicating that both $G\alpha_{16}$ and TFE3 were required for the regulation claudin 14 expression. These results are consistent with the data observed in HEK293 cells.

Up-regulation of Claudin 14 in Mouse Heart upon Pressure Overload Stress—As TFE3 and $G\alpha_{16}$ were simultaneously up-regulated in the left ventricle in the TAC model (Fig. 2), we examined whether ventricular claudin 14 was also up-regulated in the models of cardiac hypertrophy. Quantitative PCR analysis indicated that claudin 14 mRNA was increased 5-fold in the left ventricle in the TAC model but not in the isoproterenol model of cardiac hypertrophy (Fig. 7*B*), consistent with the expression profile of TFE3 and $G\alpha_{16}$ in these stimulated models (Fig. 2). Immunocytochemical analysis indicated that expression of claudin 14 was increased in the lateral membrane of cardiomyocytes rather than the intercalated disks (Fig. 7*C*). Thus, similar to our findings in cultured cells, the simultaneous up-regulation of TFE3 and $G\alpha_{16}$ was associated with gene induction of claudin 14 *in vivo* under pathologic conditions. Gene induction by $G\alpha_{16}$ and TFE3 is therefore postulated to be part of the cardiac adaptation process to pressure overload stress.

DISCUSSION

We report the identification of three MITF/TFE transcription factors, TFE3, MITF, and TFEB, as new AGS proteins selective for the $G\alpha_{16}$ subunit. These factors belong to the Myc supergene family of basic helix-loop-helix leucine zipper transcription factors that act either as a homo- or heterodimer within the family members (31–33). TFE3 formed a complex with and activated $G\alpha_{16}$ in cells. Formation of TFE3-$G\alpha_{16}$ complex resulted in the translocation of $G\alpha_{16}$ to the nucleus and up-regulation of the cell junction protein claudin 14. Expression of claudin 14 was also induced *in vivo* in the hypertrophied ventricle, and this was associated with the up-regulation of $G\alpha_{16}$ and TFE3. Thus, the transcription factor TFE3 is postulated to act as a G-protein activator for the $G\alpha_{16}$ subunit and regulate gene induction in response to pathophysiologic stress.

Although an increasing body of data implicates heterotrimeric G-proteins and their regulators as key regulators in multiple cellular events (40, 41), this is the first demonstration that activation of a $G\alpha$ subunit by an AGS drives relocalization of $G\alpha$ to the nucleus and gene transcription in mammalian cells.

Previous studies reported that heterotrimeric $G\beta_5$ translocated to the nucleus when complexed with RGS7 (16). However, the effect of RGS7-$G\beta_5$ on gene regulation has not yet been characterized. This study is the first to demonstrate a direct effect of nuclear translocation of a $G\alpha$ subunit on specific gene regulation.

The magnitude of gene induction by TFE3-$G\alpha_{16}$ was clearly dependent on the guanine nucleotide binding status of $G\alpha_{16}$ as well as the bioactivity of TFE3 for $G\alpha_{16}$ activation. Activation of $G\alpha_{16}$ in the cytosol or plasma membrane was not sufficient to induce claudin 14 expression because a constitutively active $G\alpha_{16}$ in the cytosol and plasma membrane failed to induce claudin 14 expression. Conversely, translocation of $G\alpha_{16}$ to the nucleus by the delTFE3, which lacked the ability to activate $G\alpha_{16}$, showed a blunted induction of claudin 14 as compared with intact TFE3. These observations suggest that TFE3-mediated activation of $G\alpha_{16}$ within the nucleus is essential to induce claudin 14 expression. TFE3 may serve as a direct guanine nucleotide exchange factor for $G\alpha_{16}$ upon complex formation. Alternatively, $G\alpha_{16}$ may be activated in the nucleus following removal or addition of a factor to the TFE3 complex when it is translocated into the nucleus.

The up-regulation of claudin 14 reported in this study may be an important event in remodeling of the heart following pressure overload stress. Claudin 14 was expressed in the lateral membrane of cardiomyocytes and was increased upon pressure overload stress. Claudin 14 is a member of the claudin family of more than 20 highly conserved proteins (42–44). It is interesting that the overexpression of claudin 14 induces apoptosis of cells independently of the caspase-mediated pathway (45). Moreover, in addition to its barrier function, claudin is also involved in activating pro-matrix metalloproteinase 2, which plays a role in reorganization of the extracellular matrix (46). Accordingly, the claudin-mediated sealing and/or molecular remodeling of the lateral region where cardiomyocytes are associated with the basal lamina or extracellular matrix is important for adaptation to mechanical stress. Indeed, changes in the expression of claudin 5 have been reported in the lateral membrane of cardiomyocytes in a dystrophic mouse with dilated cardiomyopathy (47, 48).

It is possible that the transcription factor MITF/TFE acts as a heterologous protein complex and binds to promoter regions to regulate the transcription of claudin 14. TFE3-$G\alpha_{16}$ may be required to assemble such a transcriptional complex, leading to increased transcription. Alternatively, TFE3-$G\alpha_{16}$ may regulate nuclear PLC-β activity and the nuclear phosphoinositide cycle independently of the plasma membrane phosphoinositide cycle influencing cell cycle and cell differentiation (49). Activation of PLC-β in the nucleus is not usually detectable in whole-cell experiments as used in this study (Fig. 4).

This is the first report of a regulatory protein for the $G\alpha_{16}$ subunit, which can be coupled to multiple GPCRs in a variety of experimental systems (37, 38). Although $G\alpha_{16}$ is enriched in hematopoietic tissue, it is also expressed in other tissues including heart (50, 51) where its expression is increased 4-fold by the cardiac stress induced in the TAC animal model. It is of particular interest to find that this multifunctional $G\alpha_{16}$ is translocated into the nucleus by a specific G-protein regulator where it plays a previously unappreciated functional role.

Various AGS proteins are involved in adaptation to various pathologic conditions (3, 20). For example, we previously identified AGS8 as a novel regulatory protein for the $G\beta\gamma$ subunit in a repetitive transient ischemia model in the rat heart (18). AGS8 was up-regulated in the myocardium by ischemic/hypoxic stress and played a critical role in hypoxia-induced apoptosis of cardiomyocytes (18, 24). Our ability to rapidly identify AGS8 and now TFE3 directly from disease-specific mRNA libraries using our yeast-based functional screen highlights its usefulness in discovering disease-specific regulatory proteins for heterotrimeric G-proteins. Such disease-specific or adaptation-specific regulatory proteins represent novel therapeutic targets in treating human diseases.

Acknowledgments—We acknowledge Dr. James R. Broach (Molecular Biology, Princeton University, Princeton, NJ) and Cadus Pharmaceutical Corp. (New York, NY) for providing yeast strains used in this study. We thank Dr. Kazuhiro Ogata (Biochemistry and Gene Regulation, Yokohama City University) for helpful comments.

REFERENCES

1. Birnbaumer, L. (2007) *Biochim. Biophys. Acta* **1768,** 772–793
2. Oldham, W. M., and Hamm, H. E. (2006) *Q. Rev. Biophys.* **39,** 117–166
3. Sato, M., Blumer, J. B., Simon, V., and Lanier, S. M. (2006) *Annu. Rev. Pharmacol. Toxicol.* **46,** 151–187
4. Cismowski, M. J. (2006) *Semin. Cell Dev. Biol.* **17,** 334–344
5. Blumer, J. B., Smrcka, A. V., and Lanier, S. M. (2007) *Pharmacol. Ther.* **113,** 488–506
6. Riddle, E. L., Schwartzman, R. A., Bond, M., and Insel, P. A. (2005) *Circ. Res.* **96,** 401–411
7. Tall, G. G., and Gilman, A. G. (2005) *Proc. Natl. Acad. Sci. U.S.A.* **102,** 16584–16589
8. Lee, M. J., and Dohlman, H. G. (2008) *Curr. Biol.* **18,** 211–215
9. Garcia-Marcos, M., Ghosh, P., and Farquhar, M. G. (2009) *Proc. Natl. Acad. Sci. U.S.A.* **106,** 3178–3183
10. Willars, G. B. (2006) *Semin. Cell Dev. Biol.* **17,** 363–376
11. Du, Q., Stukenberg, P. T., and Macara, I. G. (2001) *Nat. Cell Biol.* **3,** 1069–1075
12. Gotta, M., Dong, Y., Peterson, Y. K., Lanier, S. M., and Ahringer, J. (2003) *Curr. Biol.* **13,** 1029–1037
13. Sanada, K., and Tsai, L. H. (2005) *Cell* **122,** 119–131
14. Blumer, J. B., Kuriyama, R., Gettys, T. W., and Lanier, S. M. (2006) *Eur. J. Cell Biol.* **85,** 1233–1240
15. Shu, F. J., Ramineni, S., Amyot, W., and Hepler, J. R. (2007) *Cell. Signal.* **19,** 163–176
16. Hepler, J. R. (2005) *Sci. STKE* **2005,** pe38
17. Sato, M., Gettys, T. W., and Lanier, S. M. (2004) *J. Biol. Chem.* **279,** 13375–13382
18. Sato, M., Cismowski, M. J., Toyota, E., Smrcka, A. V., Lucchesi, P. A., Chilian, W. M., and Lanier, S. M. (2006) *Proc. Natl. Acad. Sci. U.S.A.* **103,** 797–802
19. Blumer, J. B., Lord, K., Saunders, T. L., Pacchioni, A., Black, C., Lazartigues, E., Varner, K. J., Gettys, T. W., and Lanier, S. M. (2008) *Endocrinology* **149,** 3842–3849
20. Sato, M., and Ishikawa, Y. (2010) *Pathophysiology* **17,** 89–99
21. Hendriks-Balk, M. C., Peters, S. L., Michel, M. C., and Alewijnse, A. E. (2008) *Eur. J. Pharmacol.* **585,** 278–291
22. Heximer, S. P., Srinivasa, S. P., Bernstein, L. S., Bernard, J. L., Linder, M. E., Hepler, J. R., and Blumer, K. J. (1999) *J. Biol. Chem.* **274,** 34253–34259
23. Rogers, J. H., Tamirisa, P., Kovacs, A., Weinheimer, C., Courtois, M., Blumer, K. J., Kelly, D. P., and Muslin, A. J. (1999) *J. Clin. Investig.* **104,**

567–576
24. Sato, M., Jiao, Q., Honda, T., Kurotani, R., Toyota, E., Okumura, S., Takeya, T., Minamisawa, S., Lanier, S. M., and Ishikawa, Y. (2009) *J. Biol. Chem.* **284,** 31431–31440
25. Hill, J. A., Karimi, M., Kutschke, W., Davisson, R. L., Zimmerman, K., Wang, Z., Kerber, R. E., and Weiss, R. M. (2000) *Circulation* **101,** 2863–2869
26. Cismowski, M. J., Takesono, A., Ma, C., Lizano, J. S., Xie, X., Fuernkranz, H., Lanier, S. M., and Duzic, E. (1999) *Nat. Biotechnol.* **17,** 878–883
27. Takesono, A., Cismowski, M. J., Ribas, C., Bernard, M., Chung, P., Hazard, S., 3rd, Duzic, E., and Lanier, S. M. (1999) *J. Biol. Chem.* **274,** 33202–33205
28. Cismowski, M. J., Takesono, A., Ma, C., Lanier, S. M., and Duzic, E. (2002) *Methods Enzymol.* **344,** 153–168
29. Sato, M., Ribas, C., Hildebrandt, J. D., and Lanier, S. M. (1996) *J. Biol. Chem.* **271,** 30052–30060
30. Sato, M., Kataoka, R., Dingus, J., Wilcox, M., Hildebrandt, J. D., and Lanier, S. M. (1995) *J. Biol. Chem.* **270,** 15269–15276
31. Hodgkinson, C. A., Moore, K. J., Nakayama, A., Steingrímsson, E., Copeland, N. G., Jenkins, N. A., and Arnheiter, H. (1993) *Cell* **74,** 395–404
32. Hughes, M. J., Lingrel, J. B., Krakowsky, J. M., and Anderson, K. P. (1993) *J. Biol. Chem.* **268,** 20687–20690
33. Steingrímsson, E., Copeland, N. G., and Jenkins, N. A. (2004) *Annu. Rev. Genet.* **38,** 365–411
34. Tshori, S., Gilon, D., Beeri, R., Nechushtan, H., Kaluzhny, D., Pikarsky, E., and Razin, E. (2006) *J. Clin. Investig.* **116,** 2673–2681
35. Heasley, L. E., Storey, B., Fanger, G. R., Butterfield, L., Zamarripa, J., Blumberg, D., and Maue, R. A. (1996) *Mol. Cell. Biol.* **16,** 648–656
36. Zhou, J., Stanners, J., Kabouridis, P., Han, H., and Tsoukas, C. D. (1998) *Eur. J. Immunol.* **28,** 1645–1655
37. Huang, J., and Wilkie, T. M. (2006) *UCSD-Nature Molecule Pages* 10.1038/mp.a000972.01
38. Offermanns, S., and Simon, M. I. (1995) *J. Biol. Chem.* **270,** 15175–15180
39. Wu, D., Kuang, Y., Wu, Y., and Jiang, H. (1995) *J. Biol. Chem.* **270,** 16008–16010
40. Burchett, S. A. (2003) *J. Neurochem.* **87,** 551–559
41. Spiegelberg, B. D., and Hamm, H. E. (2007) *Curr. Opin. Genet. Dev.* **17,** 40–44
42. Tsukita, S., and Furuse, M. (2002) *Curr. Opin. Cell Biol.* **14,** 531–536
43. Wilcox, E. R., Burton, Q. L., Naz, S., Riazuddin, S., Smith, T. N., Ploplis, B., Belyantseva, I., Ben-Yosef, T., Liburd, N. A., Morell, R. J., Kachar, B., Wu, D. K., Griffith, A. J., Riazuddin, S., and Friedman, T. B. (2001) *Cell* **104,** 165–172
44. Ben-Yosef, T., Belyantseva, I. A., Saunders, T. L., Hughes, E. D., Kawamoto, K., Van Itallie, C. M., Beyer, L. A., Halsey, K., Gardner, D. J., Wilcox, E. R., Rasmussen, J., Anderson, J. M., Dolan, D. F., Forge, A., Raphael, Y., Camper, S. A., and Friedman, T. B. (2003) *Hum. Mol. Genet.* **12,** 2049–2061
45. Hu, Y., Lehrach, H., and Janitz, M. (2010) *Mol. Biol. Rep.* **37,** 3381–3387
46. Miyamori, H., Takino, T., Kobayashi, Y., Tokai, H., Itoh, Y., Seiki, M., and Sato, H. (2001) *J. Biol. Chem.* **276,** 28204–28211
47. Sanford, J. L., Edwards, J. D., Mays, T. A., Gong, B., Merriam, A. P., and Rafael-Fortney, J. A. (2005) *J. Mol. Cell. Cardiol.* **38,** 323–332
48. Mays, T. A., Binkley, P. F., Lesinski, A., Doshi, A. A., Quaile, M. P., Margulies, K. B., Janssen, P. M., and Rafael-Fortney, J. A. (2008) *J. Mol. Cell. Cardiol.* **45,** 81–87
49. Irvine, R. F. (2002) *Sci. STKE* **2002,** re13
50. Wilkie, T. M., Scherle, P. A., Strathmann, M. P., Slepak, V. Z., and Simon, M. I. (1991) *Proc. Natl. Acad. Sci. U.S.A.* **88,** 10049–10053
51. Giannone, F., Malpeli, G., Lisi, V., Grasso, S., Shukla, P., Ramarli, D., Sartoris, S., Monsurró, V., Krampera, M., Amato, E., Tridente, G., Colombatti, M., Parenti, M., and Innamorati, G. (2010) *J. Mol. Endocrinol.* **44,** 259–269

Circulation Journal
Official Journal of the Japanese Circulation Society
http://www.j-circ.or.jp

REVIEW

Apoptosis in Heart Failure

– The Role of the β-Adrenergic Receptor-Mediated Signaling Pathway and p53-Mediated Signaling Pathway in the Apoptosis of Cardiomyocytes –

Takayuki Fujita, MD; Yoshihiro Ishikawa, MD

The heart works as a driving force to deliver oxygen and nutrients to the whole body. Interrupting this function for only several minutes can cause critical and permanent damage to the human body. Thus, heart failure (HF) or attenuated cardiac function is an important factor that affects both patient's the quality of life and longevity. Numerous clinical and basic studies have been performed to clarify the complex pathophysiology of HF and to develop effective therapies. Modulating the β-adrenergic receptor-mediated signaling pathway has been one of the most crucial targets for HF therapy. Impressively, recent reports identified p53, a well-known tumor suppressor, as a major player in the development of HF. The present review highlights the apoptosis of cardiomyocytes, which is one of the important mechanisms that leads to HF and can be induced by both β-adrenergic signaling and p53. Consideration of the cross-talk among these major pathways will be important when developing effective and safe therapies for HF. (*Circ J* 2011; **75:** 1811–1818)

Key Words: Adrenergic signaling; Apoptosis; Heart failure; p53

Because the heart works as a driving force to deliver oxygen and nutrients to the whole body, cardiac function is a critical factor affecting quality of life and longevity. In addition, interrupting heart function for only a few minutes can cause critical and permanent damage to the human body. A report from the United States indicated that the lifetime risk of developing congestive heart failure (HF) is approximately 20%.[1] The most common cause of HF in Western countries is coronary artery disease (CAD). Although controlling the established risk factors for CAD has become more common in general healthcare and treating with several cardioprotective agents, including β blockers, RAS inhibitors, antiplatelet agents, and statins, improves the survival rate, the current prognosis for HF is still not acceptable. Therefore, further developments in HF treatment are one of the greatest issues for extending the healthy life of humans.

Numerous clinical and basic studies have been performed to clarify the complex pathophysiology of HF. These studies have identified several mechanisms that affect cardiac function, and some therapies were developed based on these results. Many years ago, the β-adrenergic receptor (β-AR)-mediated signaling pathway was identified as one of the most important pathways that regulates cardiac function. Modulating this pathway has been one of the most crucial targets for HF therapy.[2] On the other hand, recent reports identified p53, a well-known tumor suppressor, as a major player in the development of HF.[3–5] The present review focuses on these 2 pathways.

Both pathways can induce the apoptosis of cardiomyocytes. It is well known that cardiomyocytes undergo apoptosis in response to harmful stimuli, including ischemia,[6] reperfusion,[7] oxidative stress,[8] stretching,[9] rapid pacing,[10] etc. Although some signaling mechanisms for inducing apoptosis in cardiac myocytes may be specific, such as those with Bim induction by EPAC,[11] others may be shared among different cell types. Since a 1997 report showed that failing hearts were associated with an increased number of apoptotic cardiomyocytes, the importance of apoptosis in the development of HF has been extensively examined and established in many reports.[12] The cell death of terminally differentiated cells, which cannot proliferate, directly affects tissue function. When attempting to develop an effective antiapoptotic therapy for the heart, we reviewed reports that examined the importance of each pathway in cardiomyocyte apoptosis. Based on these findings, we speculate that there is cross-talk among these pathways. Therefore, it will be important to take that into consideration when developing more effective and safe therapies.

β-AR-Mediated Apoptosis of Cardiomyocytes

The positive inotropic effect of β-AR stimulation is one of the most effective measures for maintaining cardiac output during urgent care of HF. The β-AR stimulation induces protein kinase A (PKA) activation through G protein, adenylyl

Received January 24, 2011; revised manuscript received May 18, 2011; accepted May 30, 2011; released online July 11, 2011
Cardiovascular Research Institute, Yokohama City University Graduate School of Medicine, Yokohama, Japan
Mailing address: Yoshihiro Ishikawa, MD, Cardiovascular Research Institute, Yokohama City University Graduate School of Medicine, 3-9 Fukuura, Kanazawa-ku, Yokohama 236-0004, Japan. E-mail: yishikaw@med.yokohama-cu.ac.jp
ISSN-1346-9843 doi:10.1253/circj.CJ-11-0025